Water Resources Research

RESEARCH ARTICLE
10.1029/2018WR023302

The Climatic Water Balance and Topography Control Spatial Patterns of Atmospheric Demand, Soil Moisture, and Shallow Subsurface Flow

Zachary H. Hoylman[1], Kelsey G. Jencso[1], Jia Hu[2], Zachary A. Holden[3], Justin T. Martin[4], and W. Payton Gardner[5]

[1]Montana Climate Office, W.A. Franke College of Forestry and Conservation, University of Montana, Missoula, MT, USA, [2]School of Natural Resources and the Environment, University of Arizona, Tucson, AZ, USA, [3]USDA Forest Service, Northern Region, Missoula, MT, USA, [4]Department of Ecology, Montana State University, Bozeman, MT, USA, [5]Geosciences Department, University of Montana, Missoula, MT, USA

Abstract Catchment hydrometeorology and the organization of shallow subsurface flow are key drivers of active contributing areas and streamflow generation. However, understanding how the climatic water balance and complex topography contribute to these processes from hillslope to catchment scales remains difficult. We compared time series of vapor pressure deficits and soil moisture to the climatic water balance and topographic variables across six zero-order catchments in the Lubrecht Experimental Forest (Montana, USA). We then evaluated how local hydrometeorology (volumetric water content and atmospheric vapor pressure deficit) affected the spatial occurrence of shallow subsurface flow. Generalized linear mixed model analysis revealed significant, temporally stable (monthly and seasonal average) patterns of hydrometeorology that can be predicted by the topographic wetness index and the dynamic climatic water deficit (CWD = potential evapotranspiration − actual evapotranspiration). Intracatchment patterns were significantly correlated to the topographic wetness index, while intercatchment patterns were correlated to spatiotemporal variance in the CWD during each time period. Spatial patterns of shallow subsurface flow were related to the hydrometeorological conditions of the site. We observed persistent shallow subsurface flow in convergent hillslope positions, except when a catchment was positioned in locations with high CWDs (low elevations and southerly aspects). Alternatively, we observed persistent subsurface flow across all hillslope positions (even 70-m upslope from the hollow) when catchments were positioned in locations with especially low CWDs (northerly aspects and high elevations). These results highlight the importance of considering the superposition of the catchment-scale climatic water balance and hillslope-scale topography when characterizing hydrometeorology and shallow subsurface flow dynamics.

Key Points:
- The climatic water balance and hillslope topography control spatiotemporal patterns of soil moisture and vapor pressure deficit
- Hydrometeorology explains spatiotemporal patterns of shallow subsurface flow across catchments
- The topographic organization of hydrometeorology and shallow subsurface flow is most apparent in semiarid regions

Supporting Information:
- Supporting Information S1
- Data Set S1

Correspondence to:
Z. H. Hoylman,
zachary.hoylman@umontana.edu

Citation:
Hoylman, Z. H., Jencso, K. G., Hu, J., Holden, Z. A., Martin, J. T., & Gardner, W. P. (2019). The climatic water balance and topography control spatial patterns of atmospheric demand, soil moisture, and shallow subsurface flow. *Water Resources Research*, *55*, 2370–2389. https://doi.org/10.1029/2018WR023302

Received 11 MAY 2018
Accepted 15 FEB 2019
Accepted article online 19 FEB 2019
Published online 25 MAR 2019

1. Introduction

The dominant controls on spatial patterns of moisture in the near-surface atmosphere and shallow subsurface remain poorly characterized across catchment gradients in topography and the climatic water balance. Catchments are dynamic systems, which store, transmit, and release water, but do so in spatially and temporally heterogeneous ways (McDonnell et al., 2007; Troch et al., 2009). This dynamic response is often related to the spatial distribution of moisture across topographic gradients and stochastic variability (frequency and intensity) of precipitation and energy availability that lead to shallow subsurface flow (SSF) generation (Castillo et al., 2003; Dunne & Black, 1970; Freeze, 1972; Jencso et al., 2009; Montgomery & Dietrich, 2002; Penna et al., 2011; Zhang et al., 2011).

Hydrologic fluxes occur both within and across the soil matrix-atmosphere continuum, intrinsically linking the two moisture reservoirs (Brubaker & Entekhabi, 1994; Castelli et al., 1996; Delworth & Manabe, 1989; Entekhabi et al., 1992; Entekhabi et al., 1996; Ford et al., 2015; Maxwell et al., 2007; Vivoni et al., 2007). Therefore, the moisture availability in the atmosphere and the subsurface both contribute to the average moisture states within hillslopes and across the catchments they compose. Moisture availability is driven by regional climatic processes, which are subsequently mediated by topographic gradients at various spatial and temporal scales (Carey & Woo, 2001; Maneta & Silverman, 2013; Western et al., 2004). At the catchment scale, spatially heterogeneous partitioning of climatic inputs (water and energy) is strongly influenced by topography (Chen & Kumar, 2001; Thornthwaite, 1948): gradients in orographic precipitation (Jiang,

2003; Roe, 2005) and differences in radiation on contrasting slope aspects (Bennie et al., 2008; Budyko, 1969; Fu & Rich, 2002; Oliphant et al., 2003; Shevenell, 1999). These processes drive highly complex interactions between moisture availability and net radiation, determining the partitioning of latent and sensible energy fluxes, as well as moisture transport to the subsurface across the landscape (i.e., the climatic water balance).

Climate inputs of energy and water can be further modified by hillslope topography and result in the development of microclimates across mountainous terrain (varying at scales of <1 to tens of meters). Microclimates are the fine-scale environmental conditions, which occur in localized areas close to the soil-atmosphere interface (Chen et al., 1999). Radiative and atmospheric processes that interact with topographic gradients at the hillslope scale can strongly influence microclimates. For example, the expansion of thermal energy gradients (Minder et al., 2010; Rolland, 2003), development of cold air drainage (Clements et al., 2003; Yoshino, 1984), and deflection of wind (Ruel et al., 1998) alter the water holding capacity of the air, and therefore vapor content, of the near surface atmosphere. These processes result in atmospheric microclimates that are often unique to hillslope position (e.g., convergent hillslope hollows versus sideslopes and ridgelines) and thereby alter evapotranspiration and depletion of the soil moisture reservoir.

Watershed hydrologists have long used surface topography to describe the movement of water in the subsurface in regions of considerable topographic complexity (e.g., Moore et al., 1991). This assumption is based upon the profound effect of gravity on soil water potential gradients (Dingman, 2015). Subsurface potential gradients associated with gravity in turn contribute to the dynamics of hillslope scale lateral flow (Weyman, 1973), which can be responsible for spatial patterns in soil moisture content (Grayson et al., 1997, Western et al., 1999, Western et al., 2004; but see Tromp-van Meerveld & McDonnell, 2005). However, the rate of water movement in the subsurface is highly dependent on the water content of the soil (due to highly nonlinear relationships between soil water content and hydraulic conductivity; Campbell & Norman, 2012), which varies widely across catchments. Despite this, SSF is a dominant hydrologic process that is responsible for considerable transport of water from hillslopes to streams (Jencso et al., 2009; Jencso & McGlynn, 2011; McGuire & McDonnell, 2010; Tromp-van Meerveld et al., 2015).

Although processes associated with the climatic water balance and topographic gradients are critical to understand the spatial patterns of moisture and subsurface flow across catchments (Ali et al., 2014; McGuire et al., 2005; Nippgen et al., 2015; Woods, 2003), there is a lack of field-based studies that investigate how these processes interact across space and time from plots to entire catchments. A strong correlation between topography, soil moisture, and SSF has been identified across hillslopes (Anderson & Burt, 1978; Beven & Kirkby, 1979; Burt & Butcher, 1985; Fox & Weisberg, 2011; Grayson et al., 1997; Jencso et al., 2009; McNamara et al., 2005; Troch et al., 2003; Western et al., 1998; Western et al., 1999), establishing topography as a key factor that drives catchment function. However, catchment-scale variability in the climatic water balance and hillslope scale hydrologic and atmospheric processes are rarely combined to understand the nested scales of influence leading to vapor pressure, soil moisture, and subsurface flow dynamics across catchments.

Here we bridge this knowledge gap by evaluating site hydrometeorology at different hillslope positions across six zero-order catchments spanning a large gradient in the climatic water balance. Our goal was to understand how the superposition (defined here as the spatial alignment; Williams et al., 2009) of the climatic water balance and hillslope scale topography lead to the spatial and temporal patterns of catchment moisture states. Further, we sought to quantify how the spatial organization of soil moisture and atmospheric demand impact the duration of SSF response across all catchments. Finally, we estimate potential changes in catchment-scale SSF response due to climate change.

2. Study Area

The North Fork Elk Creek (NFEC) catchment is a 17.9-km^2 headwater basin of the Columbia River that is located within the Garnet Mountain Range of Western Montana (Figure 1) at the University of Montana's Lubrecht Experimental Forest. Historical meteorological conditions have been recorded by two snow survey and telemetry (SNOTEL) stations within the NFEC catchment (Figure 1, white triangles). Mean annual temperature and precipitation for these two stations are 4.2 °C with 514 mm and 3.0 °C with 664 mm for the low elevation (Lubrecht Flume station #604 at 1,426-m elevation) and high elevation (N Frk Elk Creek station #657 at 1,905-m elevation) stations, respectively. The elevation range within the NFEC basin is 1,230–

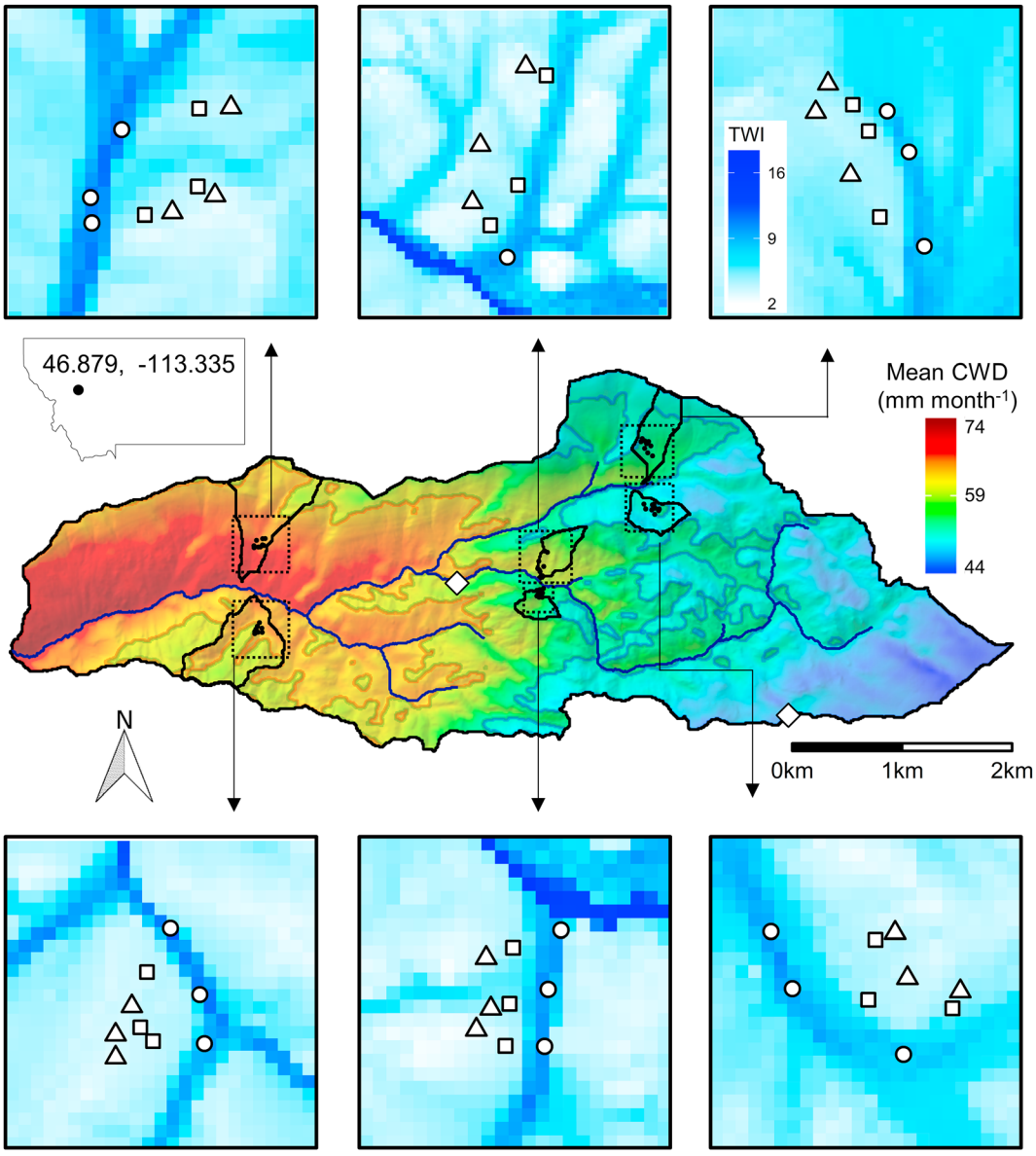

Figure 1. Map showing the location of the North Fork Elk Creek catchment within Montana, the climatic water deficit (CWD = potential evapotranspiration − actual evapotranspiration) across the North Fork Elk Creek catchment and delineated boundaries of each study catchment. Generally, the climatic water deficit decreases with increasing elevation and decreasing solar radiation. Call out plots show a map of the topographic wetness index for each study catchment and the locations of each sensor network (vapor pressure deficit, volumetric water content, and shallow subsurface flow measurements). The white circles, squares, and triangles represent hollow, sideslope, and upslope hillslope positions respectively. The dashed boxes show regions represented by call out plots. The location of SNOTEL sites within the catchment are shown by white diamonds.

2,030 m, and the stream network within the basin trends east-west. This stream network organization (E-W) has resulted in predominantly north and south facing hillsides on either side of the NFEC creek (Figure 1).

The NFEC is a snow-melt dominated catchment that stores ~46% of annual precipitation as snow at high elevations. This winter storage of precipitation causes distinct seasonality in moisture across the catchment. The NFEC is at its wettest state during and directly after snowmelt in April–May, becomes progressively drier throughout the summer (May–July), and is at its driest state in August. NFEC then becomes progressively wetter as fall rains become more abundant in September–October, after which the snowpack begins to accumulate.

Table 1
Descriptions of Variables and Symbology Used in the Manuscript

Variable	Units	Description
VPD_{mean}	kPa	Average vapor pressure deficit calculated using probes at 15 and 200 cm above the ground surface
$\overline{VPD}$	kPa	Time-averaged vapor pressure deficit calculated from the VPD_{mean} time series
θ_{5cm}	$m^3\ m^{-3}$	Volumetric water content at 5-cm depth
θ_{50cm}	$m^3\ m^{-3}$	Volumetric water content at 50-cm depth
θ_{mean}	$m^3\ m^{-3}$	Average volumetric water content between probes at 5- and 50-cm depth
$\overline{\theta}$	$m^3\ m^{-3}$	Time-averaged volumetric water content calculated from the θ_{mean} time series
HDI	kPa	The hydrometeorological dryness index calculated from the ratio of VPD_{mean} and θ_{mean}
$\overline{HDI}$	kPa	Time-averaged hydrometeorological dryness index calculated from the HDI time series
$\widehat{P}(SSF)$	$t\ t^{-1}$	Proportion of time that shallow subsurface flow was present at a given well location
$P\ (SSF\|\overline{HDI})$	NA	Probability of observing shallow sub surface flow (SSF) given the time averaged hydrometeorological dryness index value ($\overline{HDI}$) of a site

The underlying lithology of the NFEC is primarily Quartz Monzonite with small portions of the periphery along the northern catchment divide consisting of Mesoproterozoic metasedimentary mudstones and sandstones (Belt Supergroup). Soils are primarily well-drained silty loams (National Cooperative Soil Survey, U.S. Department of Agriculture, 2001). Soil depths generally vary as a function of hillslope position (median ± interquartile range for hollows and near stream zones: 1.34 m ± 0.55; sideslopes: 1.04 ± 0.42), based on 51 shallow soil well depths (Data Set S1 in the supporting information). Three coniferous tree species, *Pseudotsuga menziesii* (Douglas fir), *Pinus ponderosa* (ponderosa pine), and *Larix occidentalis* (western larch) account for ~ 80% of stems in the Lubrecht Experimental Forest (Rowell et al., 2009). The other 20% of stems are generally composed of *Pinus contorta* (lodgepole pine), *Abies lasiocarpa* (subalpine fir), and *Picea engelmannii* (Engelmann spruce).

3. Methods

3.1. General Study Design

We selected six zero-order catchments across the NFEC that capture the variability of hillslope positions and climatic water balance conditions within the basin (Figure 1). Each catchment was instrumented with nine sensor stations, consisting of three ridge, sideslope, and hollow hillslope positions along downslope hydrologic flow paths (Figure 1). Thus, there were a total of 54 stations across the catchment (three stations were excluded from the analysis due to destruction by bears). Each sensor network consisted of instruments recording local hydrometeorological conditions (volumetric soil water content and vapor pressure deficit [VPD]) and shallow groundwater wells that recorded the timing and duration of saturation, which is assumed to reflect the occurrence of SSF. For this analysis, we used a 6-month period of observation from 1 April to 30 September, which represents the transition from wettest to driest conditions across the catchment. Variables and symbols used throughout the manuscript are defined in Table 1.

3.2. Quantification of Hydrometeorological Conditions

Each hydrometeorological station within the NFEC catchment (Figure 1) was outfitted with two relative humidity (RH) and temperature (T) sensors (Aosong DHT22) and two capacitance-based volumetric water content probes (Decagon 5TE). RH and T sensors were installed in solar radiation and precipitation shields at 15 and 200 cm above the ground surface. The volumetric water content probes were installed at 5- and 50-cm depths below the soil surface (θ_{5cm} and θ_{50cm}; $m^3\ m^{-3}$ Figure 2). These sensors were connected to a custom built, printed circuit board-data logger that was powered by a 12v 4 Ah battery and charged by a solar panel and a voltage regulator (SunGaurd 4.5A 12v Solar Charge Controller). Data were recorded every 30 min. Above ground atmospheric demand for moisture was represented by the VPD (kPa):

$$\mathrm{VPD} = e_t - \left(e_t * \frac{\mathrm{RH}}{100}\right)$$

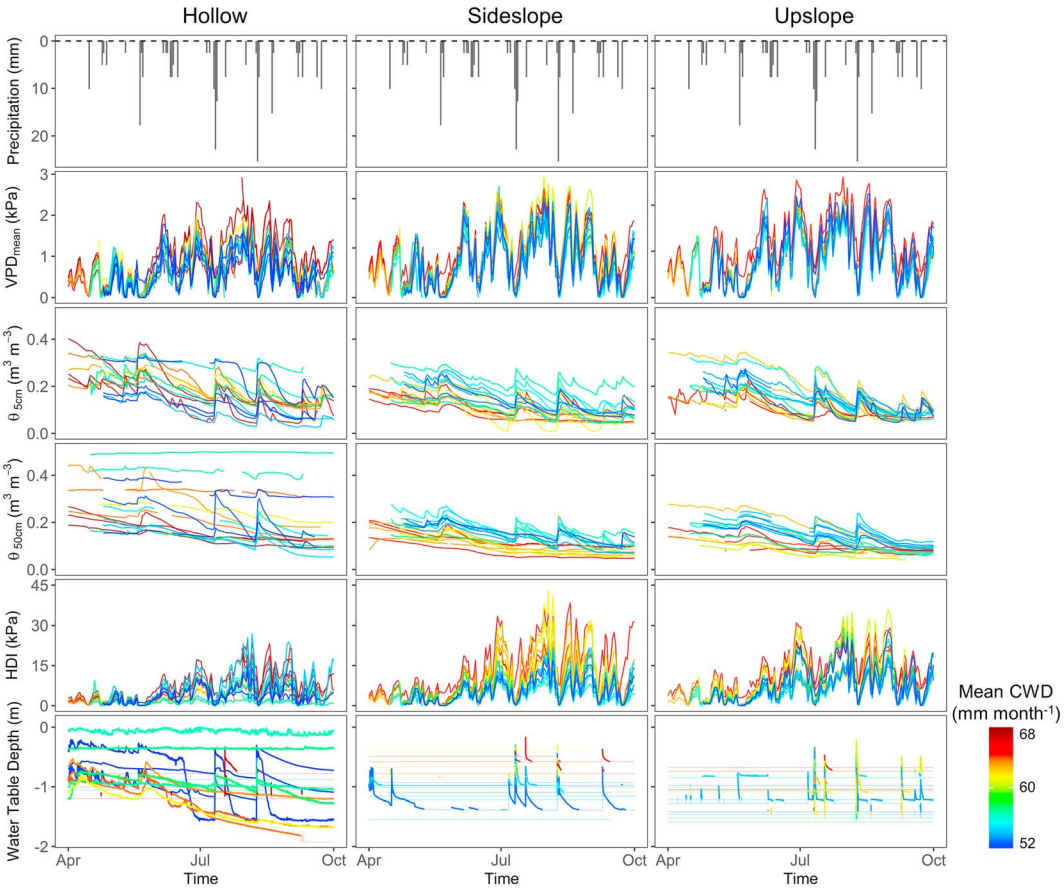

Figure 2. Plots representing data collected in the North Fork Elk Creek from 1 April to 30 September of 2016 separated by hillslope position (hollow, sideslope, and upslope). Each panel represents precipitation, mean vapor pressure deficit from probes at 15 cm and 200 cm above the surface (VPD_{mean}; kPa), soil moisture at 5- and 50-cm depths (θ_{5cm}, θ_{50cm} respectively, $m^3\ m^{-3}$), the hydrometeorological dryness index (HDI; kPa), and water table depth below ground (m) for each sensor station. Each time series is color coded by the mean monthly climatic water deficit of a site.

where e_t is the saturation vapor pressure and RH is the relative humidity in percent. The saturation vapor pressure was calculated according to Tetens (1930):

$$e_t = 0.6108^* \exp\left(\frac{17.27^*T}{(T+237.3)}\right)$$

where T is the temperature. The mean VPD (VPD_{mean}; Figure 2) was subsequently calculated by averaging the recorded VPD at 15 and 200 cm for each sensor network location and time step (30 min).

We calculated volumetric water content from dielectric permittivity following Topp et al. (1980) using the manufacturer's suggested equation. This paired soil moisture probe design contributed to a more accurate representation of the soil moisture conditions throughout the soil profile. For each station, the mean volumetric water content (θ_{mean}) was calculated by averaging θ_{5cm} and θ_{50cm} for each sensor location and time step (30 min).

In addition to the hydrometeorological stations described above, we installed shallow groundwater wells at each sensor network location (Figure 1). These wells were used to assess how spatial patterns of site hydrometeorology contributed to SSF dynamics. Wells were installed with a solid steel rod, inserted into the screened PVC casing, and driven to refusal, which is assumed to be at the bedrock-soil interface. Wells consisted of 3.8-cm diameter PVC pipe screened across the entire depth. At the surface, all wells were sealed with a bentonite slurry. Water levels were measured every hour across the well network using either TruTrack Inc. capacitance rods or Solinst pressure transducers (Levelogger model 3001).

For each well we calculated the proportion of observations where saturation, and thus SSF, occurred ($\widehat{P}(\mathrm{SSF})$) to inform a model describing the probability of SSF for a given sensor network location. The proportion of observations where SSF occurred for each well was estimated as

$$\widehat{P}(\mathrm{SSF}) = \left(\frac{\mathrm{Observations_{WW}}}{\mathrm{Observations_{Total}}}\right)$$

where $\mathrm{Observations_{WW}}$ represents the number of observations where water was present in the well and $\mathrm{Observations_{Total}}$ represents the total number of observations recorded between 1 April and 30 September. We also characterized hourly precipitation using data from the Lubrecht Flume SNOTEL (604), which was subsequently summed for each day to calculate daily precipitation amount.

3.3. Hydrometeorological Dryness Index

To describe the combined hydrometeorological conditions in the near-surface atmosphere and soil, we calculated the hydrometeorological dryness index (HDI; kPa) following Martin et al. (2017). We used the HDI because it integrates both above and below ground moisture conditions, representing the moisture supply and demand at a site. The HDI also serves as a simple proxy for the driving force of water flow across the soil-plant-atmosphere continuum (Martin et al., 2017; Sperry et al., 2003), although it is not our intent to model the moisture flux across this gradient. HDI was calculated as:

$$\mathrm{HDI} = \frac{\mathrm{VPD_{mean}}}{\theta_{\mathrm{mean}}}$$

where the $\mathrm{VPD_{mean}}$ is the mean VPD (of the paired VPD probes at each site) and θ_{mean} is the mean volumetric water content (of the paired soil moisture probes at each site) for each recorded time step. Therefore, for each sensor network location we computed half hourly time series of the HDI (Figure 2).

For each sensor location we calculated the time-averaged mean volumetric water content ($\overline{\theta}$), VPD ($\overline{VPD}$), and HDI ($\overline{HDI}$) for the season as a whole (seasonal average; 1 April to 30 September), and for each month individually. $\overline{\theta}$ and $\overline{VPD}$ represent the average moisture storage and demand of the site respectively. $\overline{HDI}$ represents the average hydrometeorological conditions for a given location. Low values of $\overline{HDI}$ indicate wet conditions, which arise when atmospheric demand ($\overline{VPD}$) is small and soil moisture content ($\overline{\theta}$) is high. Alternatively, large values of $\overline{HDI}$ represent dry conditions, which arise when atmospheric demand is large and when soil moisture content is low.

3.4. Quantification of Catchment Topography

We selected the topographic wetness index (TWI) to characterize the topographic influence on soil moisture across the NFEC. The TWI accounts for two topographic controls on water movement; the specific drainage area contributing to a hillslope position and the local slope (Beven & Kirkby, 1979). The TWI was derived as a similarity index to describe shallow soil moisture and groundwater levels (Beven & Kirkby, 1979; Detty & McGuire, 2010; Grayson et al., 1997; Jencso et al., 2009; Rinderer et al., 2014; Seibert et al., 2003; Western et al., 1999) but has also been correlated with ecological processes such as forest carbon accumulation and productivity (Hoylman et al., 2018; Swetnam et al., 2017).

To calculate the TWI, we used a 1-m^2 digital elevation model (DEM) derived from light detection and ranging acquisitions for the catchment that were obtained in June of 2005 (Horizons Inc., Rapid City, South Dakota). DEM pixel sizes were resampled to 10-m resolution in order to eliminate microtopographic features, which are unlikely to influence subsurface redistribution and microclimatic conditions (e.g., logs and surficial boulders). Using the SAGA GIS platform (Conrad et al., 2015), the TWI was calculated as

$$\mathrm{TWI} = \ln\left(\frac{\alpha}{\tan(\beta)}\right)$$

where a is the specific upslope accumulated area for a given point in the catchment and β is the local slope. For the upslope area calculation we used the triangular multiple direction flow algorithm (Seibert & McGlynn, 2007).

3.5. Gridded Water Balance Data

We characterized catchment-scale climatically driven moisture and energy availability using a simple daily soil water balance model, created at 8-arc second (~250-m) resolution and subsequently downscaled to 30 m by thin plate spline regression (Nychka et al., 2017). This model is a highly simplified representation of climatically driven water availability; it was not our intent to represent the precise magnitude of the water balance of the NFEC, rather we used this dynamic index to quantify relative differences in seasonal water availability across the watershed. Due to the simplicity of this vertical water balance model, lateral flow, bedrock leakage, or variability in vegetation cover are not considered in the water balance calculations. We incorporate the effects of lateral flow by using the TWI in conjunction with this water balance model. These limitations certainly add error to the water balance model; however, we suggest that this approach is a more accurate representation of climatic conditions compared to using static measures alone (such as annual insolation and/or elevation grids).

In the model, the soil at each grid cell was treated as a single layer whose depth was defined by a soil water holding capacity extracted from the SSURGO database. Incoming precipitation was stored in the soil and treated as saturation excess runoff when storage was exceeded. Vegetation was assumed to be a uniform grass cover, and water loss from the soil (via evapotranspiration) was estimated using the Penman-Monteith formulation, following methods provided by the Food and Agriculture Organization (FAO; Allen et al., 1998). Daily snowpack accumulation and melt were estimated using an empirical model driven by daily temperature, radiation (corrected for cloud cover, slope, and aspect), and precipitation (Holden et al., 2018). Inputs to the model included daily solar radiation and temperature (Holden et al., 2016), daily minimum and maximum RH (Holden et al., 2018), daily 4-km resolution precipitation (Abatzoglou, 2013), and wind speed from the North American Regional Reanalysis (Mesinger et al., 2006). We generated daily data for the NFEC for 2016, estimating potential evapotranspiration (PET), actual evapotranspiration (AET), and the unmet demand, or the climatic water deficit (CWD = PET-AET) for each time step. Daily CWD grids were then summed for each month to produce total cumulative monthly CWD grids at 250-m resolution.

3.5.1. Downscaling to 30-m Resolution

We used a secondary downscaling approach to more finely resolve the elevation and insolation mediated variations in the soil water balance. Using a 30-m DEM to correct for terrain geometry (e.g., shading of direct radiation by adjacent terrain and slope/aspect adjustment of radiation intensity), we calculated monthly mean clear-sky (cloud-free) radiation from 1 April to 30 September using the SOLPET6 algorithm (Flint & Childs, 1987; Flint & Flint, 2008). These grids were then combined to produce a monthly mean clear-sky radiation grid. This radiation and elevation data serve as a physical template for mapping the radiation and elevation variability within the 250-m CWD data. We then used thin plate spline regression, implemented in the R computing language with the library fields (R Core Team, 2017, Nychka et al., 2017), to estimate the CWD for each month as a function of solar radiation and elevation. Here we extracted a sample of 1,000 CWD grid cells with their underlying elevation and radiation, fit the regression, and then predicted the fitted model back to the 30-m grids. The resulting 30-m CWD maps retain the scale and spatial properties of the original 250-m data, but with additional topographic detail that is more closely aligned with the scale of the TWI data.

3.6. Assessment of Site Hydrometeorology

To quantify the relative roles of landscape topography and the climatic water balance on the spatial variability of hydrometeorology, we fit generalized linear mixed models (GLMMs, lme4 R package; Bates et al., 2014) to each response variable ($\overline{\theta}$, $\overline{VPD}$, and $\overline{HDI}$) for the season and during individual months. A GLMM framework was used for our modeling efforts to account for nonnormal data distributions and to account for random effects across study catchments (Bolker et al., 2009; McCulloch & Neuhaus, 2001). For these response variables, each GLMM assumes a gamma distribution (bound by 0 and ∞), which utilizes a log link. In each GLMM we included a catchment identifier which we used as a random effect term (see call-out maps in Figure 1, which show the six catchments) to account for catchment specific variability, which was not driven by the fixed effect variables (TWI, CWD, and an interaction term [TWI:CWD]).

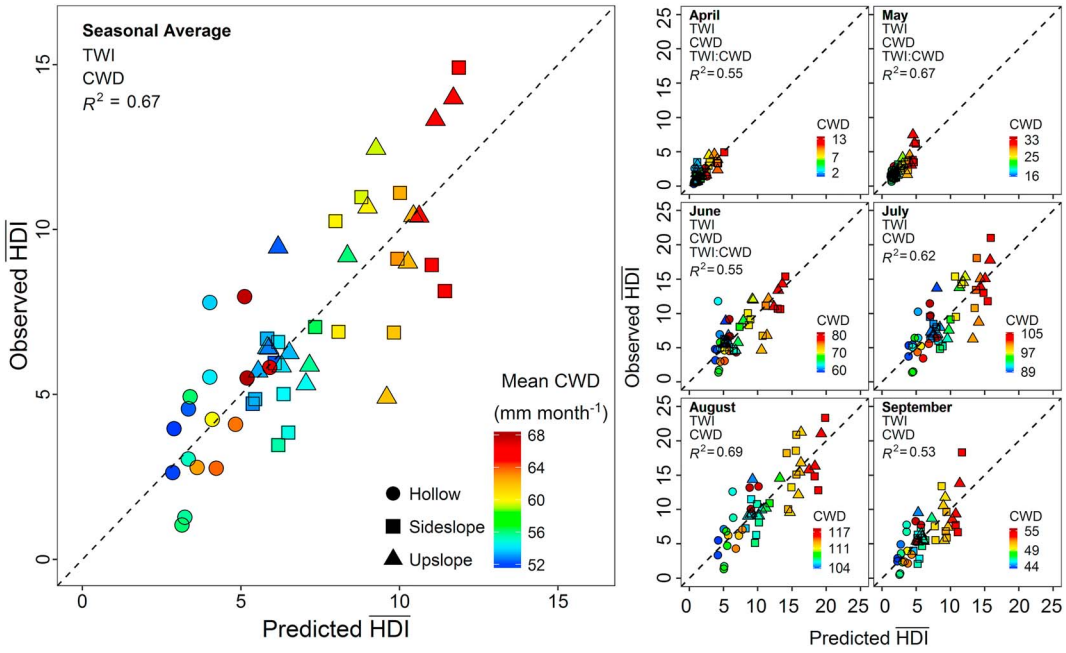

Figure 3. Generalized linear mixed model predicted mean hydrometeorological dryness index ($\overline{HDI}$; ratio of vapor pressure deficit and volumetric soil water content) and the observed $\overline{HDI}$ values for each sensor location and time period. Conditions become progressively wetter (lower $\overline{HDI}$) in increasingly convergent hillslope positions (larger topographic wetness indexes [TWIs]) and as the climatic water deficit (CWD) decreases. The wettest conditions occur where convergent terrain and low climatic water deficits align. The time period considered (seasonal and monthly) and variables selected for each model are shown in the top left corner of each plot. Colors represent the monthly climatic water deficit at the sensor location for the time period considered, and symbol shape represents the hillslope position for each sensor location. R^2 values were calculated using observed and predicted $\overline{HDI}$ values.

We used these GLMMs to assess the explanatory power of the fixed effect terms only (random effects were not used in any prediction) on spatiotemporal patterns of $\overline{\theta}$, $\overline{VPD}$, and $\overline{HDI}$ (Figure 3 and Table 2). We report the population averaged model (only fixed effects) for each response variable and time period in Table 2. Similarly, for all predictions (such as in Figures 3, 5, and 6), we used only the model's fixed effects. We used the Akaike information criterion (AIC) to select the best model (i.e., which terms were included in each model) to describe spatial patterns of each response variable (Venables & Ripley, 2002; Wagenmakers & Farrell, 2004). For each fixed effect term we conducted an analysis of deviance significance test, presented as p-values, using a Type II (when no interaction terms were present) or Type III (when interaction terms were present) Wald χ^2 test (Table S1; car R package, Fox & Weisberg, 2011). After fitting each model we calculated the coefficient of determination (R^2) to assess the variance explained by the cumulative effect of the fixed effect model terms.

3.7. Assessment of SSF

In a similar fashion to the models described above, we quantified the relationship between seasonal average moisture conditions of a site ($\overline{\theta}$, $\overline{VPD}$, and $\overline{HDI}$ as predictor variables) and the seasonal probability of saturation ($\widehat{P}$(SSF)) using three independent GLMMs. This allowed us to evaluate how site moisture state (either volumetric water content, VPD, or the combined hydrometeorological conditions) affected the probability of observing a shallow groundwater table, and thus subsurface flow. All three of these GLMMs assumed a binomial distribution and utilized a logit link, appropriate for modeling probability using proportions of grouped observations where groups represent observations from a single well time series. In the GLMMs we included a catchment identifier, which was considered a random effect term to account for catchment specific variation in subsurface flow dynamics (such as differences in bedrock percolation). The GLMMs considered $\overline{\theta}$, $\overline{VPD}$, and $\overline{HDI}$ for each site as a fixed effect to represent the universal influence of site moisture state and hydrometeorology on subsurface flow dynamics. This allowed us to approximate the population average probability of SSF with respect to the fixed effect terms (i.e., P [SSF|$\overline{HDI}$] for example). The general form

Table 2
Time-Averaged Volumetric Water Content ($\overline{\theta}$; $m^3\ m^{-3}$), Vapor Pressure Deficit ($\overline{VPD}$; kPa), and Hydrometeorological Dryness Index ($\overline{HDI}$; kPa) Generalized Linear Mixed Model (GLMM) Fixed Effect Coefficients and R^2 for Each Time Period Considered

Variable	Time period	Intercept	TWI	CWD	TWI: CWD	R^2
$\overline{\theta}$						
	Seasonal Average	−0.810	0.091	−0.028	NA	0.416
	April	−1.904	0.076	−0.030	NA	0.466
	May	−1.548	0.073	−0.022	NA	0.428
	June	−0.524	0.084	−0.026	NA	0.377
	July	0.596	0.095	−0.033	NA	0.375
	August	1.810	0.101	−0.041	NA	0.377
	September	−0.947	0.114	−0.042	NA	0.354
$\overline{VPD}$						
	Seasonal Average	−1.025	−0.032	0.017	NA	0.375
	April	−1.265	NA	NA	NA	NA
	May	−1.754	0.042	0.044	−0.003	0.463
	June	0.030	NA	NA	NA	NA
	July	−1.181	−0.027	0.015	NA	0.300
	August	1.037	−0.512	−0.007	0.004	0.552
	September	−0.589	−0.254	0.003	0.004	0.351
$\overline{HDI}$						
	Seasonal Average	−0.234	−0.117	0.048	NA	0.672
	April	−0.027	−0.045	0.185	−0.007	0.553
	May	−0.592	0.039	0.084	−0.005	0.667
	June	−1.745	0.136	0.061	−0.003	0.552
	July	−1.594	−0.113	0.046	NA	0.618
	August	−3.901	−0.116	0.063	NA	0.688
	September	−1.496	−0.124	0.082	NA	0.534

Note. Each GLMM assumes a gamma distribution with a log link function. All coefficients are reported in log space. NA, not available.

of each GLMM described above is presented in the Supporting Information Document S1 (equations (S1) and (S2)).

3.8. Out-of-Sample Model Validation

We evaluated the out-of-sample predictive power and coefficient stability of each model used for spatial prediction using a Monte Carlo cross-validation approach. Here we randomly selected 60% of the data set to train a model and used the remaining 40% to test the model. We ran the Monte Carlo cross-validation simulation 2600 times. For each iteration, we refit the GLMM to the training data set, used the estimated fixed effect coefficients to estimate the values of the testing data set, and subsequently calculated the predictive power (R^2) for each model. We also stored each model's fixed effect coefficient estimates to evaluate the coefficient stability of the model.

3.9. Catchment-Scale Hydrometeorology and SSF

We calculated spatial estimates of the hydrometeorological conditions across the NFEC using the seasonal population average models for $\overline{HDI}$ and P (SSF|$\overline{HDI}$). The $\overline{HDI}$ model used gridded data sets of TWI and the CWD as input data sets to approximate the spatial distribution of hydrometeorological conditions across the basin. The resultant $\overline{HDI}$ grid was then used as an input data set to calculate the spatial distribution of SSF probability given $\overline{HDI}$ (i.e., P [SSF|$\overline{HDI}$]).

To examine how values of $\overline{HDI}$ and P (SSF|$\overline{HDI}$) varied within discrete zones of the climatic water balance, we separated the NFEC catchment into three regions with equal areas (high, moderate, and low CWD tertiles), as determined by the seasonal mean monthly CWD for April–September 2016 (Figure 1). Generally, regions of high CWD (>61.8 mm; Figure 1, red lines) were located at low elevations along southerly aspects, whereas regions of low CWD (<52.9 mm; Figure 1, blue lines) were located at high elevations along northerly aspects. All other spatial regions are considered moderate CWD regions (61.8–52.9 mm; Figure 1, green lines). For each spatial prediction and each climatic water balance region, we generated empirical cumulative distribution functions (CDF) to evaluate the general behavior of $\overline{HDI}$ and P (SSF|$\overline{HDI}$) values with respect to the climatic water balance.

3.10. Potential Climate Change Impacts on SSF

We approximated potential changes in SSF in the NFEC due to climate change by estimating the spatial distribution of SSF under more arid climatic conditions. We accomplished this by applying a 15% increase to the observed CWD distribution for the NFEC. This increase represents a reasonable, albeit very simple, approximation for CWD conditions in the midcentury (2040–2060; see Anderegg et al., 2015). We then applied the seasonal average $\overline{HDI}$ model to the new CWD grid to obtain an estimate of the $\overline{HDI}$ conditions for the midcentury. Next we calculated the change in SSF as a function of the new $\overline{HDI}$ grid (ΔP [SSF|$\overline{HDI}$]) by subtracting the current SSF estimates from the SSF estimates from the 15% CWD increase scenario. While this is a reasonable approximation of potential changes to CWD due to climate change, linear extrapolation such as this does not incorporate nonlinear and asymptotic behaviors in future CWD conditions; there is uncertainty in this estimate.

4. Results

4.1. Topographic and CWD Impacts on Local Hydrometeorology

The TWI and CWD were selected as significant predictors of $\overline{\theta}$ (Table 2) for each time period (seasonal average and individual months). The TWI and the CWD were also selected to model $\overline{VPD}$ for each time period, except for April and June (where no predictors were selected, for example, AIC was lowest with only the

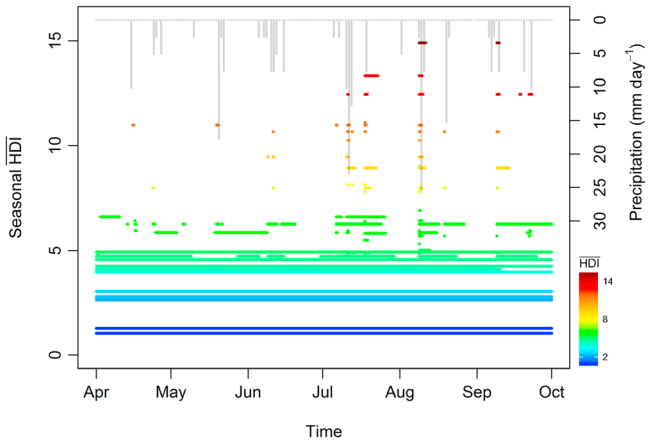

Figure 4. Binary plot showing the observed seasonal time averaged hydrometeorological dryness index ($\overline{HDI}$) value and the period of shallow subsurface flow for each well across the North Fork Elk Creek catchment. The colored lines represent periods of saturation, assumed to be shallow subsurface flow, in each well with respect to the $\overline{HDI}$ for that location (colors also represent the $\overline{HDI}$ value). A hyetograph representing a time series of rainfall at the Lubrecht Flume SNOTEL (#604) is presented on the inverted y axis. Generally, locations with wet hydrometeorological conditions (low $\overline{HDI}$) had persistent shallow subsurface flow, while more arid locations (high $\overline{HDI}$) exhibited transient shallow subsurface flow dynamics when sufficient precipitation occurred.

intercept term; Table 2). Similar to $\overline{\theta}$, the TWI and the CWD were selected to model $\overline{HDI}$ (Table 2 and Figure 3) for every time period. An interaction term between TWI and the CWD (TWI:CWD) was also selected as an important predictor for May, August, and September for the monthly $\overline{VPD}$ GLMMs and the April, May, and June $\overline{HDI}$ GLMMs (Table 2). This multiplicative interaction describes a differential effect of TWI on $\overline{VPD}$ and $\overline{HDI}$ as a function of the CWD.

Generally, as values of TWI increased (transitioning from ridgelines and planar slope positions to convergent hillslope positions), $\overline{\theta}$ increased while the $\overline{VPD}$ and $\overline{HDI}$ decreased. As the CWD became less arid (transitioning from low elevation south aspects to high elevation north aspects), $\overline{\theta}$ tended to increase while $\overline{VPD}$ and $\overline{HDI}$ tended to decrease. The wettest locations (largest $\overline{\theta}$ and smallest $\overline{VPD}$ and $\overline{HDI}$) occurred where convergent hillslope positions and locations of low CWD (high elevation and north aspect) were aligned in space. Further investigation to the behavior of the $\overline{HDI}$ seasonal average model revealed that the difference in $\overline{HDI}$ between hollow and upslope hillslope positions increased as the CWD became more arid (discussed further below, see Figure 7a for reference).

4.2. Hydrometeorological Conditions and SSF

Qualitative evaluation of $\overline{HDI}$ at each site and the magnitude of precipitation (mm/day) revealed differences in the amount of precipitation required to initiate and sustain SSF (Figure 4). Large precipitation events (20 mm/day) in mid-July and mid-August were sufficient to cause SSF in almost all of the wells in the catchment, even those in dry $\overline{HDI}$ locations (Figure 4, dark red lines). However, SSF in these dry $\overline{HDI}$ locations tended to be highly transient and occurred for short durations (i.e., hours to days). Conversely, in locations with moderate $\overline{HDI}$ (such as Figure 4, green lines), SSF occurred during relatively small precipitation events and was sustained for long durations (i.e., days to weeks). In locations of particularly wet $\overline{HDI}$ (Figure 4, blue lines), SSF persisted for the duration of the study period.

We quantified the relationship between $\overline{HDI}$ and $\widehat{P}(SSF)$ using a binomial GLMM (Figure 5 regression line, intercept = 6.948, fixed effect $\overline{HDI}$ coefficient = −1.505, both in logit space). The R^2 value for this relationship was 0.64, and the p-value of the $\overline{HDI}$ coefficient was <0.05 using a Type II Wald χ^2 test. We also evaluated the relationships between $\overline{\theta}$ and $\overline{VPD}$ on seasonal $\widehat{P}(SSF)$ independently, but the $\overline{HDI}$ model preformed the best (AIC was 56239.3, 78778.2, and 118274.5 for models using $\overline{HDI}$, $\overline{\theta}$, and $\overline{VPD}$ respectively).

We used the significant relationship between $\overline{HDI}$ and $\widehat{P}(SSF)$ to estimate the space and time variability of SSF across the larger NFEC catchment. In general, hillslope hollows (Figure 5, circles) had longer durations of SSF than sideslope and upslope positions (Figure 5, squares and triangles respectively). Similar to the $\overline{HDI}$, the superposition of topography and the climatic water balance determined the spatial and temporal occurrence of SSF across the NFEC. P (SSF|$\overline{HDI}$) values were close to 0 in zones of high CWD (Figure 5, red and orange symbols), even in areas with very large TWI values (e.g., large drainage areas with low local slope, Figure 5, red circles). As the CWD decreased and climatic water balance conditions became wetter (e.g., high elevation and northerly aspects), the duration of SSF increased. Long periods of SSF occurred within hollow hillslope positions with large contributing areas (Figure 5, blue circles), as well as along steep sideslope and upslope positions with very small contributing areas (Figure 5, blue triangles and squares) when the catchment was positioned in regions of low CWD (high elevation and northerly aspect).

4.3. Assessment of Predictive Power

Both the $\overline{HDI}$ and P (SSF |$\overline{HDI}$) models performed well when predicting out-of-sample testing data sets. The median ± interquartile range of the prediction R^2 of the 2,600 runs was 0.66 ± 0.15 for the $\overline{HDI}$ model and 0.61 ± 0.23 for the P (SSF|$\overline{HDI}$) model (Figure S1). The median ± interquartile range of the TWI and CWD

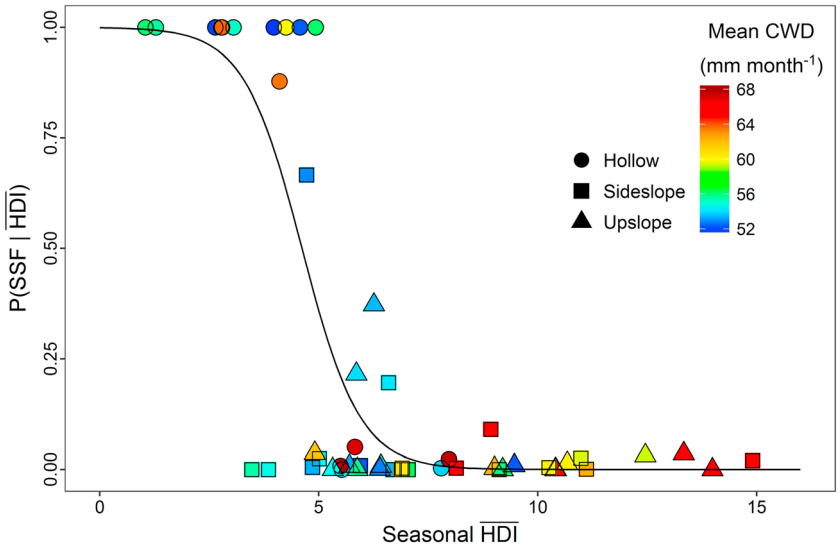

Figure 5. Plot showing the generalized linear mixed model used to quantify the relationship between the seasonal $\overline{HDI}$ and the probability of shallow subsurface flow (SSF) at each well location. Colors represent the mean monthly climatic water deficit, and symbols represent the hillslope position for each sensor location. Generally, locations with lower $\overline{HDI}$ values have a higher probability of longer durations of shallow subsurface flow response.

estimates were -0.118 ± 0.021 and 0.047 ± 0.011, respectively, for the $\overline{HDI}$ model (which were very similar to the estimates obtained when fitting the model with the entire data set; Figure 3 and Table 2). The median $\pm$ interquartile range of the $\overline{HDI}$ model estimates for the P (SSF|$\overline{HDI}$) model was -1.65 ± 0.64 (which were also very similar to the estimates obtained when fitting the model with the entire data set; Figure 5). This result indicates that both models that were ultimately used to predict the catchment scale patterns of $\overline{HDI}$ and P (SSF|$\overline{HDI}$) were reasonable models for spatial analysis. However, the validation of these models was constrained to the conditions observed across the six study catchments and therefore uncertainty beyond these conditions is larger.

4.4. Catchment-Scale Estimates of Hydrometeorology and Saturation

We evaluated CDFs for catchment scale estimates of $\overline{HDI}$ and P (SSF|$\overline{HDI}$) across discrete zones of the CWD. The CDF curves for $\overline{HDI}$ (Figure 6a) emphasized that the spatial variability of $\overline{HDI}$ was related to the CWD (e.g., larger tails of the CDF are found in drier climatic water balance regions indicating greater spatial variability). We also observed that the CWD shifted the $\overline{HDI}$ values toward wetter or drier conditions, which was expected given the CWD model coefficients (Table 2). It is important to note that slight differences in the TWI and CWD distributions for each climatic water balance tertile contributed to the variability in the CDF distribution for $\overline{HDI}$. About 50% of the catchment area had $\overline{HDI} < 9.81$, 6.79, and 4.60 kPa for high, moderate, and low CWDs, respectively.

CDFs of (P [SSF|$\overline{HDI}$]; Figure 6b) for each climatic water balance tertile illustrate the dramatic effect the CWD has on the occurrence of SSF in the NFEC. In high CWD regions (Figure 6b, red line), very large drainage areas with low slopes were required to initiate SSF; however, SSF was highly transient and occurred for short durations. In zones of moderate CWD (Figure 6b, green line), hillslope positions with sufficiently large drainage areas and low slopes (TWI) were more likely to sustain SSF. In locations of low CWD (Figure 6b, blue line), saturation was likely across most hillslope positions, even far upslope and on ridgelines. For each climatic water balance tertile, 50% of the catchment area had P (SSF|$\overline{HDI}$) values of <0.001, 0.036, and 0.503 for high, moderate, and low CWDs, respectively.

To further investigate the behavior of $\overline{HDI}$ as a function of the TWI and CWD, we interpolated the seasonal average $\overline{HDI}$ model for a gradient of TWI values between 2.5 and 12.5 and across a range of CWD values (Figure 7a). The TWI values represent hillslope-scale topographic characteristics of zero-order catchments, while the CWD values represent observed and potential climatic water balance conditions for the NFEC

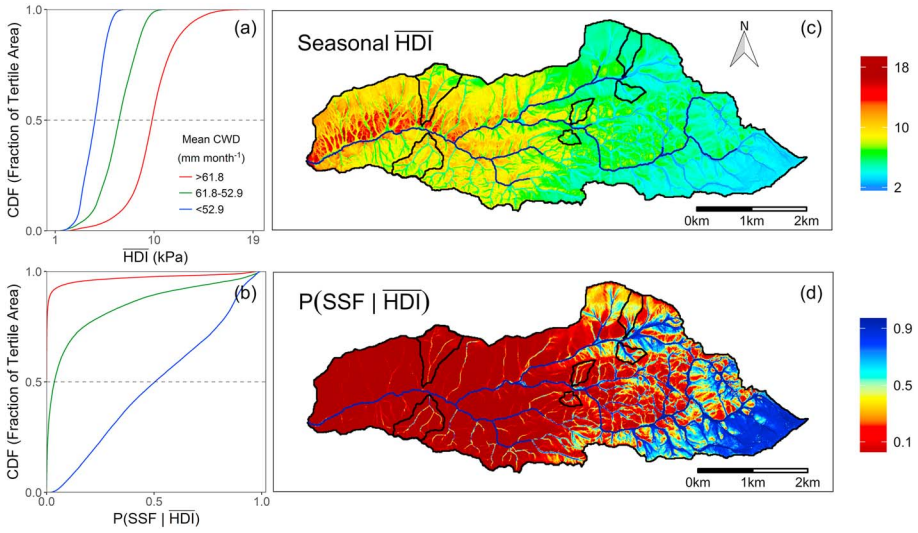

Figure 6. Cumulative distribution functions (CDFs) and spatial estimates of the (a and c) mean seasonal hydrometeorological dryness index ($\overline{HDI}$) and the (b and d) probability of shallow subsurface flow (P [SSF|$\overline{HDI}$]) for the North Fork Elk Creek catchment. The line colors on each CDF plot represent pixels falling within each tertile of the deficit (>61.8 mm, 61.8–52.9 mm, and <52.9 mm are red, green, and blue respectively).

(potential conditions assume a 15% increase). We also include the values of $\overline{HDI}$ where the probability of SSF was 0.95, 0.50, and 0.05 (Figure 7a; P [SSF|$\overline{HDI}$], dashed lines). In general, the difference between hollow and ridge hillslope positions (i.e., $\Delta\overline{HDI}$ for TWI values of 2.5 and 12.5) is relatively large in high CWD regions and becomes progressively smaller as the CWD decreased. Similarly, an equivalent change in the observed CWD range (43.4–74.1 mm) caused $\overline{HDI}$ to vary substantially for upslope and ridgeline hillslope positions (TWI = 2.5) but caused relatively little change for more convergent hillslope positions (TWI = 12.5).

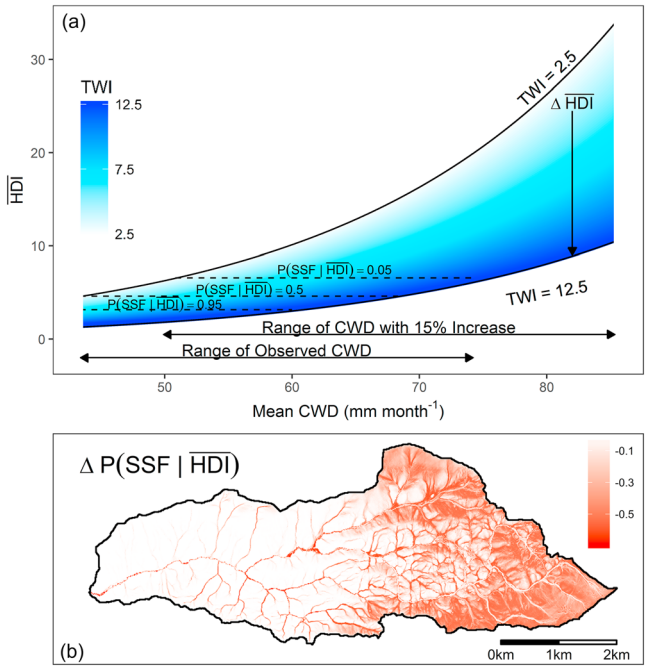

Figure 7. (a) Generalized linear mixed model estimates of mean seasonal hydrometeorological dryness index ($\overline{HDI}$) as a function of the topographic wetness index (TWI; color ramp) and the mean monthly climatic water deficit (CWD). The dashed lines represent the $\overline{HDI}$ values that correspond with 5, 50, and 95% shallow subsurface flow probabilities. (b) Map showing the change in shallow subsurface flow probability (ΔP [SSF|$\overline{HDI}$]) given a 15% increase in the observed climatic water deficit.

Finally, using an approximation of the potential climate change impacts on the CWD for the mid-century (15% CWD increase, Figure 7a), we calculated the predicted change in SSF for the NFEC (ΔP [SSF|$\overline{HDI}$]; Figure 7 b). Generally, the largest changes in P (SSF|$\overline{HDI}$) occurred where low CWD promoted SSF along upslope hillslope positions. Locations with large drainage areas and low slopes had an attenuated response to increases in the climatic aridity, and as a result, were characterized by smaller reductions in P (SSF|$\overline{HDI}$) than nearby upslope counterparts.

5. Discussion

Our results confirm that the hydrometeorology of the NFEC catchment is highly influenced by hillslope-scale topographic convergence and divergence and catchment-scale gradients in the climatic water balance (Figure 3). These findings suggest that the superposition of hillslope scale topography and the climatic water balance need to be considered when describing spatial and temporal patterns of hydrometeorology within complex terrain. We observed consistently wetter conditions in the subsurface and atmosphere in convergent hillslope positions across all study catchments. Hydrometeorology varied significantly along upslope hillslope positions across the CWD gradient in our 17.9-km^2 catchment; from relatively wet in locations with low CWD to relatively dry in locations with high CWD (Figure 7a). This effect was also important for hillslope hollows; however, the magnitude of change was significantly smaller

(Figure 7a). This result demonstrates the nested scales of influence and the relative effect of hydrologic redistribution and the climatic water balance that determine the dynamic organization of moisture across a catchment.

The superposition of the climatic water balance and topography had a particularly significant effect on the spatial patterns of SSF in the NFEC. Catchment positions with large drainage areas and low local slopes located within areas of large CWDs (i.e., catchments at low elevation and southerly facing) were characterized by short and highly transient saturation events, if saturation occurred at all (Figures 4 and 5). Conversely, when catchments were located in areas with small CWDs (i.e., catchments at high elevation and northerly facing slopes) saturation events occurred frequently and for longer durations across all hillslope positions, even far upslope from the convergent hollow (~70-m upslope from the adjacent hollow). Our results suggest that characterizing vapor pressure, soil moisture, and SSF along gradients of topography and the climatic water balance is critical for scaling and transferring process understanding of subsurface flow dynamics across catchments.

5.1. Spatiotemporal Patterns of Soil Moisture

We observed significant spatial organization of soil moisture across the NFEC catchment, which was relatively consistent through time (Table 2). The relative magnitude of soil moisture for a catchment as a whole (intercatchment) was driven by catchment-scale gradients in the climatic water balance, while the moisture of each site (intracatchment) was highly influenced by hillslope-scale convergence and divergence (Figure 2). This reflects the hierarchical controls on soil moisture, which originate from the climatic water (and energy) balance and are subsequently altered by hydrologic and atmospheric processes operating across zones of hillslope topographic convergence and divergence (represented by the TWI).

The intercatchment patterns of soil moisture related to the CWD in the NFEC provide further evidence of the strong influence of the climatic water balance on spatial patterns of soil moisture (Table 2). Our results align with Langston et al. (2015), who showed that snowmelt dynamics on north versus south facing slopes produced higher sustained soil moisture on north facing slopes (lower CWD than southerly facing slopes) despite similar snowpacks. Williams et al. (2009) also showed the important influence of aspect and slope on soil moisture patterns in a snow-dominated semiarid watershed in Idaho.

The topographic controls on moisture patterns for our study were more persistent and spatially organized than those described in several other studies (e.g., Burt & Butcher, 1985; Grayson et al., 1997; McNamara et al., 2005). This result is in contrast to the preferential states hypothesis of Grayson et al. (1997), which posits that soil moisture patterns are organized along hillslope topographic gradients (drainage lines) only when SSF processes are active; during the wet portion of the season. We observed greater volumetric water contents in convergent positions along hillslope drainage lines (spatially organized along the TWI) even in sites where SSF was almost entirely absent throughout the season (Table 2). This may reflect enhanced soil moisture due to the downslope movement of water in the unsaturated zone or the cumulative effect of microclimates on soil moisture (such as reduced VPDs, reduced wind speeds, reduced radiation exposure, and therefore smaller evaporative fluxes) in convergent zones.

In a forested catchment in Maryland, Tenenbaum et al. (2006) observed strong and temporally persistent soil moisture along convergent hillslope topography under both wet and dry moisture conditions. Our results support this finding and indicate strong intracatchment- and intercatchment-scale patterns in soil moisture regardless of moisture state, even during the driest time periods. These results support research describing temporal stability of soil moisture patterns (Gómez-Plaza et al., 2000; Grant et al., 2004; Kachanoski & Jong, 1988; Mohanty & Skaggs, 2001; Tenenbaum et al., 2006), although we demonstrate that the relative volumetric water content across catchments varies as a function of the climatic water balance. While some of this stability in moisture may be attributed to soil properties (i.e., Grant et al., 2004; Lin, 2006), our results suggest that the topographic organization of microclimate (VPD; Western et al., 2004) in conjunction with the occurrence of SSF (similar to mechanisms attributed to the wet state spatial organization in Grayson et al., 1997) are both important. We suggest that the degree and temporal consistency of observed topographic organization of soil moisture highly depends on the scale of observation (e.g., plot, hillslope or catchment scale) and the density of observations across sites (Tenenbaum et al., 2006).

Our CWD approach did not account for potential differences in transpiration rates that are a significant component of the water balance in NFEC due to the variation in density, species, and phenology of vegetation along hillslope flow paths (Looker et al., 2018). Root water uptake associated with the spatial distribution of vegetation influences soil moisture (Renner et al., 2016) and the expansion and contraction of active catchment contributing areas (Nippgen et al., 2015). Hoylman et al. (2018) reported greater total forest biomass and longer periods of vegetation greenness (a proxy for photosynthetic activity) in convergent hillslope positions in the NFEC. Greater photosynthetic activity in convergent hillslope positions promotes greater rates of transpiration (Hawthorne & Miniat, 2018), and ultimately causes reductions in soil moisture in convergent positions. These considerations would contribute to unexplained variance in our $\overline{HDI}$ model and uncertainty in our CWD model. However, we hypothesize that the upslope subsidies of moisture via SSF pathways and the microclimate of convergent hillslope positions is sufficient to offset large transpiration-related moisture reductions in convergent hillslope positions relative to sideslope and ridgeline positions.

5.2. Spatiotemporal Patterns of Vapor Pressure Deficits

We observed considerable organization of atmospheric vapor pressure across the NFEC catchment (Table 2) that was similar to the subsurface moisture patterns, although spatial correlations were slightly weaker than for soil moisture (seasonal $\overline{\theta}$ $R^2 = 0.42$; seasonal $\overline{VPD}$ $R^2 = 0.38$; Table 2). Atmospheric VPDs tended to become smaller in convergent locations with high TWI values, as well as in regions with wet climatic water balance conditions (lower CWD). This organization is representative of the mutual interactions between soil moisture and atmospheric vapor that determine the partitioning of latent and sensible heat fluxes (Entekhabi et al., 1996; Gu et al., 2006), as well as topographic controls on atmospheric turbulence via topographic deflection of wind (Ruel et al., 1998). Reductions in wind speed in convergent hillslope positions decrease the potential for the near-surface atmosphere to redistribute moist air parcels to the bulk air above the canopy, increasing the RH. There is also likely a biotic component, such that vegetation can modify wind speeds and solar radiation below canopies (Campbell & Norman, 2012; Chen et al., 1999; De Frenne et al., 2013), influencing the temperature, water holding capacity, and evaporative flux of the near-surface atmosphere (Royer et al., 2012). The combined effect of vegetative and topographic deflection of wind, radiation sheltering by conifer canopies, and increased moisture content of the soil all likely contribute to the observed organization of VPD across gradients in the TWI.

5.3. Patterns of Hydrometeorology

We combined a measure of atmospheric demand ($\overline{VPD}$) and soil moisture ($\overline{\theta}$) into a simple index (HDI; Martin et al., 2017) in order to better describe the hydrometeorological conditions of the near-surface atmosphere and soil. In semiarid forests, VPD affects rates of soil water evaporation and therefore soil moisture contents in the top 5 cm of the soil zone (Raz-Yaseef et al., 2012). Soil moisture content influences the matric potential of the soil surface, affecting infiltration and percolation of precipitation into the soil column (Campbell & Norman, 2012). This atmospheric influence would not be captured by soil moisture probes positioned in the shallow soil column (such as 5 cm below the O/A horizon), especially when organic litter is present above the mineral soil. By combining the atmospheric demand with soil moisture we suggest that a better representation of near-surface hydrometeorological moisture availability is obtained.

Similar to our findings of the spatiotemporal organization of soil moisture across the NFEC, we saw considerable temporal consistency in the spatial organization of local hydrometeorology (Table 2 and Figure 3). Topographic controls on hydrometeorology have been observed before, with elevation imparting the primary control (Vivoni et al., 2007); our results highlight the strong influence of hillslope scale topography. However, our research design was considerably different to previous studies, primarily due to the spatial density of our network with a focus on both climatic controls (similar to those reported by Vivoni et al., 2007) and hillslope scale topographic gradients. Our results in conjunction with the results of Vivoni et al. (2007) provide evidence of the nested scales of influence on site hydrometeorology, controlled hierarchically by climate, and topographically controlled hydrologic processes.

An intriguing result emerged from modeling $\overline{HDI}$ continuously across gradients in TWI and the CWD. Specifically, the relative difference in hydrometeorology between sideslope and hollow hillslope positions ($\Delta\overline{HDI}$; Figure 7a) varied based on the CWD. The greatest values of $\Delta\overline{HDI}$ (13 kPa) for the observed CWD range occurred in regions with the driest climatic water balance conditions (Figures 1; 3, red symbols; and

7a), which was remarkably larger than that of the wettest climatic water balance regions (3.3 kPa). This key result shows that hillslope-scale topography becomes an increasingly important driver of variability in hydrometeorology (e.g., the difference in hydrometeorology between hillslope positions within a catchment is greater) as landscapes transition from relatively wet to relatively dry climatic water balance conditions. This result can be extrapolated across time, suggesting that hillslope topography may attenuate changes in hydrometeorological moisture availability as climate change increases aridity in regions such as the Western U.S.

5.4. Hydrometeorology and Subsurface Flow

The antecedent moisture condition of a site is an important factor contributing to the occurrence of SSF in steep catchments with well drained soils (Dunne & Black, 1970; Freeze, 1972; James & Roulet, 2009; Penna et al., 2011; Sidle et al., 2000) because the amount of water needed (e.g., snowmelt or rainfall) to achieve saturation, and therefore SSF, is conditional on the amount of moisture in the soil pore spaces prior to water input. Although intuitive, this theoretical framework provides a powerful method to describe where SSF is likely to occur in catchments with spatially variable moisture conditions due to topography and gradients in the climatic water balance. Indeed, in the NFEC, the duration and probability of SSF was highly related to the average moisture state of a site (Figures 4 and 5).

The hydrometeorological conditions of a site were more effective at describing the variability in the occurrence of SSF across the NFEC than subsurface (volumetric water content) or atmospheric (VPD) conditions alone. This result suggests that incorporating both atmospheric and subsurface moisture conditions is important to describe the hydrologic response of a catchment. Often the relationship between moisture conditions and hillslope runoff are threshold driven (e.g., Penna et al., 2011), representing fundamental transitions between capillary and gravity driven drainage processes (Maneta et al., 2008; Torres et al., 1998; Weyman, 1973). We observed a clear transition between sites where saturation was absent or present, which corresponded with the hydrometeorological gradient of the catchment (occurring between $\overline{HDI}$ values of 7–4 kPa). This finding agrees with several studies that highlighted the dominant control of site moisture on hillslope runoff dynamics (Castillo et al., 2003; Hrnčíř et al., 2010; Mosley, 1982; Penna et al., 2011; Woods et al., 1997; Woods & Rowe, 1996) and suggests that active zones of SSF are highly sensitive to small changes in vapor pressures and soil moisture.

Generally hillslope positions with large contributing areas and low slopes had a more frequent and persistent occurrence of SSF than sideslope and upslope locations. However, describing the probability of SSF with hillslope position alone does not capture the spatial complexity of this important hydrologic response at the catchment scale. This is due to the strong contribution of the climatic water balance in determining the hydrometeorological conditions of the site (Figures 3 and 7a and Table 2), and the large spatial variability of climatic forcing across catchments (Thornthwaite, 1948). Large areas of sustained SSF were largely restricted to zones of low CWD (Figures 5 and 6b and 6d). Based on our spatial predictions (Figure 6d), we found that ~19% of the catchment had saturation probabilities greater than 0.5 (P [SSF|$\overline{HDI}$)] > 0.5), and ~79% of that proportion occurred in regions of CWD < 52.9 mm/month, such as high elevation northerly aspects. This suggests that the majority of streamflow generation via hillslope connectivity pathways (see Jencso et al., 2009, McGuire & McDonnell, 2010, and Tromp-van Meerveld et al., 2015, for information on hillslope-stream connectivity) occurs where the CWD is low. This has significant implications for potential changes to the source areas of streamflow in semiarid headwater catchments due to the sensitivity of hillslope areas to changes in the CWD. For example, using this modeling framework and projections of future changes to the climatic water balance (see Anderegg et al., 2015, for examples of CWD projections into 2100), estimates of catchment-scale streamflow generation resilience to climate change may be obtained (discussed below).

5.5. Broader Implications

This study provides unique insights on the nested scales of influence of hydrologic processes across hillslopes and larger catchments. We highlight that the superposition of the climatic water balance and hillslope topography is critical to consider in order to understand hydrometeorology in complex terrain (Figure 7a). The method employed in this study provides a transferable approach to estimate hydrometeorological conditions across gradients of topographic complexity (i.e., catchments with highly dendritic morphology versus

relatively low relief planar morphology) and contrasting climate. This simple approach is transferable due to the quantification of the dynamic climatic water balance (which incorporates the temporal and spatial heterogeneity in water and energy inputs), in conjunction with our detailed understanding of the role of topography in mediating microclimate and moisture redistribution. We also provide a framework for understanding the spatial occurrence of SSF due to the strong influence of hydrometeorology.

Understanding how source areas of streamflow may respond to climate change is a primary concern for watershed managers and practitioners around the world. Estimating temporal changes to active sources areas of stream flow (Nippgen et al., 2015; Tague et al., 2009) represents a powerful method to evaluate potential climate change impacts on catchment runoff. As an example, we applied a 15% increase to the observed CWD (Figures 7a and 7b) in order to quantify potential climate change impacts on the spatial extent of dominant streamflow source areas across the NFEC. While simple, this climate change estimate is a reasonable and conservative approximation of potential changes in the water balance by the mid-century. Significant reductions of SSF in the low CWD regions of the basin (e.g., high elevation and northerly aspects), which exceeded a 50% reduction in some locations (Figure 7b, scaled between 0 and 1), suggest that catchments in semiarid environments are extremely sensitive to changes in the climatic water balance. However, locations with large, convergent drainage areas have more attenuated responses to climate change, representing regions of hydrologic resistance for streamflow generation (Figures 7a and 7b). Nevertheless, the large spatial reduction of areas with active SSF is likely to cause considerable reductions in headwater discharge and may have implications beyond SSF. For example, groundwater recharge in these basins may be severely affected by these changes in soil moisture and SSF, greatly impacting vital groundwater resources downslope.

This study also has implications for understanding fine-scale patterns in ecohydrology (Rodriguez-Iturbe, 2000) and ecosystem sensitivity to climate change (Dobrowski, 2011). Fine spatial scale patterns of hydrometeorology are emerging as important drivers of variable conifer growth rates (Martin et al., 2017), due to the strong influence of soil-atmosphere moisture gradients on xylem water potentials and therefore intraannual ecosystem productivity dynamics. Our results suggest that vegetation in convergent hillslope positions with large drainage areas will have a greater capacity to buffer regional climate change due to the impact of microclimate and SSF (providing upslope hydrological subsidies to downslope positions) on moisture availability. This result provides further physical evidence of the occurrence of spatial patterns of microrefugia in complex terrain (Dobrowski, 2011; McLaughlin et al., 2017). While topographic patterns of vegetation structure and productivity have been observed in many environments (Flores Cervantes et al., 2014; Hoylman et al., 2018; Hwang et al., 2012; Ivanov et al., 2008; Swetnam et al., 2017), we provide direct, field-based evidence of the atmospheric and subsurface processes likely to drive such patterns. Regions of microrefugia should be protected to promote biological adaptation to climate (Morelli et al., 2016) and provide pathways of ecosystem connectivity to assist in the natural migration of species to more favorable climatic locations (Krosby et al., 2010).

6. Conclusions

Site hydrometeorology is determined by processes that operate across catchment to subhillslope spatial scales. Within one semiarid catchment, we quantified these nested scales of influence, measuring hydrometeorology (soil moisture and VPDs) and shallow subsurface flow dynamics across gradients of hillslope position (intracatchment) and the climatic water balance continuum (intercatchment). We found strong relationships linking these climatic and hydrologic processes, demonstrating the importance of the superposition of the climatic water balance and complex topography on moisture availability. Intracatchment topographic gradients (e.g., hillslope position) were especially important for determining site hydrometeorology when catchments were located within particularly arid portions of the climatic water balance continuum (e.g., low elevation and southerly aspects). Conversely, intracatchment patterns became less important in determining hydrometeorology when catchments were positioned in the hydric portion of the climatic water balance continuum (e.g., high elevation and northerly aspects). We found that SSF was almost entirely absent in the arid regions across the basin (even in areas with very large, convergent drainage areas) but persistently occurred across both convergent and upslope positions (~70 m from the adjacent hollow) in hydric regions of the catchment. Finally, we observed a strong spatial organization of

SSF as a function of local hydrometeorology, emphasizing the dominant role of moisture conditions in driving hydrologic connectivity.

Acknowledgments
This work was made possible by a USDA NIFA McIntire Stennis award 233327 to Jencso, NSF grants DEB-1457749 and DEB-1457720 to Jencso and Hu, and by a NASA applied science program Wildland Fire award (agreement NNH11ZDA001N-FIRES) awarded to Holden. Additional support was provided by NSF EPSCoR through the Montana Institute on Ecosystems. The authors appreciate extensive logistic support from the staff of the Lubrecht Experimental Forest, especially Forest Manager, Frank Maus. We would like to thank the anonymous reviewers for their thoughtful comments and suggestions, which improved this manuscript. Data used for the analyses presented in this manuscript are available in Data Set S1.

References

Abatzoglou, J. T. (2013). Development of gridded surface meteorological data for ecological applications and modelling. *International Journal of Climatology*, *33*(1), 121–131. https://doi.org/10.1002/joc.3413

Ali, G., Birkel, C., Tetzlaff, D., Soulsby, C., McDonnell, J. J., & Tarolli, P. (2014). A comparison of wetness indices for the prediction of observed connected saturated areas under contrasting conditions. *Earth Surface Processes and Landforms*, *39*(3), 399–413. https://doi.org/10.1002/esp.3506

Allen, R. G., Pereira, L. S., Raes, D., & Smith, M. (1998). Crop evapotranspiration—Guidelines for computing crop water requirements-FAO Irrigation and drainage paper 56. *FAO, Rome*, *300*(9), D05109.

Anderegg, W. R., Flint, A., Huang, C. Y., Flint, L., Berry, J. A., Davis, F. W., et al. (2015). Tree mortality predicted from drought-induced vascular damage. *Nature Geoscience*, *8*(5), 367–371. https://doi.org/10.1038/ngeo2400

Anderson, M. G., & Burt, T. P. (1978). The role of topography in controlling throughflow generation. *Earth Surface Processes and Landforms*, *3*(4), 331–344. https://doi.org/10.1002/esp.3290030402

Bates, D., Mächler, M., Bolker, B., & Walker, S. (2014). Fitting linear mixed-effects models using lme4. arXiv preprint arXiv: 1406.5823.

Bennie, J., Huntley, B., Wiltshire, A., Hill, M. O., & Baxter, R. (2008). Slope, aspect and climate: Spatially explicit and implicit models of topographic microclimate in chalk grassland. *Ecological Modelling*, *216*(1), 47–59. https://doi.org/10.1016/j.ecolmodel.2008.04.010

Beven, K. J., & Kirkby, M. J. (1979). A physically based, variable contributing area model of basin hydrology/Un modèle à base physique de zone d'appel variable de l'hydrologie du bassin versant. *Hydrological Sciences Journal*, *24*(1), 43–69. https://doi.org/10.1080/02626667909491834

Bolker, B. M., Brooks, M. E., Clark, C. J., Geange, S. W., Poulsen, J. R., Stevens, M. H. H., & White, J. S. S. (2009). Generalized linear mixed models: A practical guide for ecology and evolution. *Trends in Ecology & Evolution*, *24*(3), 127–135. https://doi.org/10.1016/j.tree.2008.10.008

Brubaker, K. L., & Entekhabi, D. (1994). Nonlinear dynamics of water and energy balance in land-atmosphere interaction. Ralph M. Parsons Lab. Tech. Rep. 341, Massachusetts Institute of Technology.

Budyko, M. I. (1969). The effect of solar radiation variations on the climate of the Earth. *Tellus*, *21*(5), 611–619.

Burt, T. P., & Butcher, D. P. (1985). Topographic controls of soil moisture distributions. *European Journal of Soil Science*, *36*(3), 469–486. https://doi.org/10.1111/j.1365-2389.1985.tb00351.x

Campbell, G. S., & Norman, J. M. (2012). *An introduction to environmental biophysics*. Berlin, Germany: Springer Science & Business Media.

Carey, S. K., & Woo, M. K. (2001). Spatial variability of hillslope water balance, Wolf Creek basin, subarctic Yukon. *Hydrological Processes*, *15*(16), 3113–3132. https://doi.org/10.1002/hyp.319

Castelli, F., Rodriguez-Iturbe, I., & Entekhabi, D. (1996). An analytical framework for the modelling of the spatial interaction between the soil moisture and the atmosphere. *Journal of Hydrology*, *184*(1–2), 19–34. https://doi.org/10.1016/0022-1694(95)02966-4

Castillo, V. M., Gomez-Plaza, A., & Martınez-Mena, M. (2003). The role of antecedent soil water content in the runoff response of semiarid catchments: A simulation approach. *Journal of Hydrology*, *284*(1–4), 114–130. https://doi.org/10.1016/S0022-1694(03)00264-6

Chen, J., & Kumar, P. (2001). Topographic influence on the seasonal and interannual variation of water and energy balance of basins in North America. *Journal of Climate*, *14*(9), 1989–2014. https://doi.org/10.1175/1520-0442(2001)014<1989:TIOTSA>2.0.CO;2

Chen, J., Saunders, S. C., Crow, T. R., Naiman, R. J., Brosofske, K. D., Mroz, G. D., et al. (1999). Microclimate in forest ecosystem and landscape ecology: Variations in local climate can be used to monitor and compare the effects of different management regimes. *Bioscience*, *49*(4), 288–297. https://doi.org/10.2307/1313612

Clements, C. B., Whiteman, C. D., & Horel, J. D. (2003). Cold-air-pool structure and evolution in a mountain basin: Peter Sinks, Utah. *Journal of Applied Meteorology*, *42*(6), 752–768. https://doi.org/10.1175/1520-0450(2003)042<0752:CSAEIA>2.0.CO;2

Conrad, O., Bechtel, B., Bock, M., Dietrich, H., Fischer, E., Gerlitz, L., et al. (2015). System for Automated Geoscientific Analyses (SAGA) v. 2.1.4. *Geoscientific Model Development*, *8*, 1991–2007. https://doi.org/10.5194/gmd-8-1991-2015

Core Team, R. (2017). *R: A language and environment for statistical computing*. Vienna, Austria: R Foundation for Statistical Computing. 2016

De Frenne, P., Rodríguez-Sánchez, F., Coomes, D. A., Baeten, L., Verstraeten, G., Vellend, M., et al. (2013). Microclimate moderates plant responses to macroclimate warming. *Proceedings of the National Academy of Sciences*, *110*(46), 18,561–18,565. https://doi.org/10.1073/pnas.1311190110

Delworth, T., & Manabe, S. (1989). The influence of soil wetness on near-surface atmospheric variability. *Journal of Climate*, *2*(12), 1447–1462. https://doi.org/10.1175/1520-0442(1989)002<1447:TIOSWO>2.0.CO;2

Detty, J. M., & McGuire, K. J. (2010). Topographic controls on shallow groundwater dynamics: Implications of hydrologic connectivity between hillslopes and riparian zones in a till mantled catchment. *Hydrological Processes*, *24*(16), 2222–2236. https://doi.org/10.1002/hyp.7656

Dingman, S. L. (2015). *Physical hydrology*. Prentice Hall, New York: Waveland press.

Dobrowski, S. Z. (2011). A climatic basis for microrefugia: The influence of terrain on climate. *Global Change Biology*, *17*(2), 1022–1035. https://doi.org/10.1111/j.1365-2486.2010.02263.x

Dunne, T., & Black, R. D. (1970). Partial area contributions to storm runoff in a small New England watershed. *Water Resources Research*, *6*(5), 1296–1311. https://doi.org/10.1029/WR006i005p01296

Entekhabi, D., Rodriguez-Iturbe, I., & Bras, R. L. (1992). Variability in large-scale water balance with land surface-atmosphere interaction. *Journal of Climate*, *5*(8), 798–813. https://doi.org/10.1175/1520-0442(1992)005<0798:VILSWB>2.0.CO;2

Entekhabi, D., Rodriguez-Iturbe, I., & Castelli, F. (1996). Mutual interaction of soil moisture state and atmospheric processes. *Journal of Hydrology*, *184*(1–2), 3–17. https://doi.org/10.1016/0022-1694(95)02965-6

Flint, A. L., & Childs, S. W. (1987). Calculation of solar radiation in mountainous terrain. *Agricultural and Forest Meteorology*, *40*(3), 233–249. https://doi.org/10.1016/0168-1923(87)90061-X

Flint, L. E., & Flint, A. L. (2008). A basin-scale approach to estimating stream temperatures of tributaries to the Lower Klamath River, California. *Journal of Environmental Quality*, *37*(1), 57–68. https://doi.org/10.2134/jeq2006.0341

Flores Cervantes, J. H., Istanbulluoglu, E., Vivoni, E. R., Holifield Collins, C. D., & Bras, R. L. (2014). A geomorphic perspective on terrain-modulated organization of vegetation productivity: Analysis in two semiarid grassland ecosystems in southwestern United States. *Ecohydrology*, *7*(2), 242–257. https://doi.org/10.1002/eco.1333

Ford, T. W., Quiring, S. M., Frauenfeld, O. W., & Rapp, A. D. (2015). Synoptic conditions related to soil moisture-atmosphere interactions and unorganized convection in Oklahoma. *Journal of Geophysical Research: Atmospheres*, *120*, 11,519–11,535. https://doi.org/10.1002/2015JD023975

Fox, J., & Weisberg, S. (2011). *An R companion to applied regression*. Thousand Oaks, California: Sage Publications.

Freeze, R. A. (1972). Role of subsurface flow in generating surface runoff: 1. Base flow contributions to channel flow. *Water Resources Research*, *8*(3), 609–623. https://doi.org/10.1029/WR008i003p00609

Fu, P., & Rich, P. M. (2002). A geometric solar radiation model with applications in agriculture and forestry. *Computers and Electronics in Agriculture*, *37*(1–3), 25–35. https://doi.org/10.1016/S0168-1699(02)00115-1

Gómez-Plaza, A., Alvarez-Rogel, J., Albaladejo, J., & Castillo, V. M. (2000). Spatial patterns and temporal stability of soil moisture across a range of scales in a semi-arid environment. *Hydrological Processes*, *14*(7), 1261–1277. https://doi.org/10.1002/(SICI)1099-1085(200005)14:7<1261::AID-HYP40>3.0.CO;2-D

Grant, L., Seyfried, M., & McNamara, J. (2004). Spatial variation and temporal stability of soil water in a snow-dominated, mountain catchment. *Hydrological Processes*, *18*(18), 3493–3511. https://doi.org/10.1002/hyp.5798

Grayson, R. B., Western, A. W., Chiew, F. H., & Blöschl, G. (1997). Preferred states in spatial soil moisture patterns: Local and nonlocal controls. *Water Resources Research*, *33*(12), 2897–2908. https://doi.org/10.1029/97WR02174

Gu, L., Meyers, T., Pallardy, S. G., Hanson, P. J., Yang, B., Heuer, M., et al. (2006). Direct and indirect effects of atmospheric conditions and soil moisture on surface energy partitioning revealed by a prolonged drought at a temperate forest site. *Journal of Geophysical Research*, *111*, D16102. https://doi.org/10.1029/2006JD007161

Hawthorne, S., & Miniat, C. F. (2018). Topography may mitigate drought effects on vegetation along a hillslope gradient. *Ecohydrology*, *11*(1), e1825. https://doi.org/10.1002/eco.1825

Holden, Z. A., Swanson, A., Klene, A. E., Abatzoglou, J. T., Dobrowski, S. Z., Cushman, S. A., et al. (2016). Development of high-resolution (250 m) historical daily gridded air temperature data using reanalysis and distributed sensor networks for the US Northern Rocky Mountains. *International Journal of Climatology*, *36*(10), 3620–3632. https://doi.org/10.1002/joc.4580

Holden, Z. A., Swanson, A., Luce, C. H., Jolly, W. M., Maneta, M., Oyler, J. W., et al. (2018). Decreasing fire season precipitation increased recent western US forest wildfire activity. *Proceedings of the National Academy of Sciences*, *115*(36), E8349–E8357. https://doi.org/10.1073/pnas.1802316115

Hoylman, Z. H., Jencso, K. G., Hu, J., Martin, J. T., Holden, Z. A., Seielstad, C. A., & Rowell, E. M. (2018). Hillslope topography mediates spatial patterns of ecosystem sensitivity to climate. *Journal of Geophysical Research: Biogeosciences*, *123*, 353–371. https://doi.org/10.1002/2017JG004108

Hrnčíř, M., Šanda, M., Kulasová, A., & Císlerová, M. (2010). Runoff formation in a small catchment at hillslope and catchment scales. *Hydrological Processes*, *24*(16), 2248–2256. https://doi.org/10.1002/hyp.7614

Hwang, T., Band, L. E., Vose, J. M., & Tague, C. (2012). Ecosystem processes at the watershed scale: Hydrologic vegetation gradient as an indicator for lateral hydrologic connectivity of headwater catchments. *Water Resources Research*, *48*, W06514. https://doi.org/10.1029/2011WR011301

Ivanov, V. Y., Bras, R. L., & Vivoni, E. R. (2008). Vegetation-hydrology dynamics in complex terrain of semiarid areas: 1. A mechanistic approach to modeling dynamic feedbacks. *Water Resources Research*, *44*, W03429. https://doi.org/10.1029/2006WR005588

James, A. L., & Roulet, N. T. (2009). Antecedent moisture conditions and catchment morphology as controls on spatial patterns of runoff generation in small forest catchments. *Journal of Hydrology*, *377*(3–4), 351–366. https://doi.org/10.1016/j.jhydrol.2009.08.039

Jencso, K. G., & McGlynn, B. L. (2011). Hierarchical controls on runoff generation: Topographically driven hydrologic connectivity, geology, and vegetation. *Water Resources Research*, *47*, W12528. https://doi.org/10.1029/2011WR010666

Jencso, K. G., McGlynn, B. L., Gooseff, M. N., Wondzell, S. M., Bencala, K. E., & Marshall, L. A. (2009). Hydrologic connectivity between landscapes and streams: Transferring reach-and plot-scale understanding to the catchment scale. *Water Resources Research*, *45*, W04428. https://doi.org/10.1029/2008WR007225

Jiang, Q. (2003). Moist dynamics and orographic precipitation. *Tellus A*, *55*(4), 301–316. https://doi.org/10.1034/j.1600-0870.2003.00025.x

Kachanoski, R. G., & Jong, E. (1988). Scale dependence and the temporal persistence of spatial patterns of soil water storage. *Water Resources Research*, *24*(1), 85–91. https://doi.org/10.1029/WR024i001p00085

Krosby, M., Tewksbury, J., Haddad, N. M., & Hoekstra, J. (2010). Ecological connectivity for a changing climate. *Conservation Biology*, *24*(6), 1686–1689. https://doi.org/10.1111/j.1523-1739.2010.01585.x

Langston, A. L., Tucker, G. E., Anderson, R. S., & Anderson, S. P. (2015). Evidence for climatic and hillslope-aspect controls on vadose zone hydrology and implications for saprolite weathering. *Earth Surface Processes and Landforms*, *40*(9), 1254–1269.

Lin, H. (2006). Temporal stability of soil moisture spatial pattern and subsurface preferential flow pathways in the Shale Hills Catchment. *Vadose Zone Journal*, *5*(1), 317–340. https://doi.org/10.2136/vzj2005.0058

Looker, N., Martin, J., Hoylman, Z., Jencso, K., & Hu, J. (2018). Diurnal and seasonal coupling of conifer sap flow and vapour pressure deficit across topoclimatic gradients in a subalpine catchment. *Ecohydrology*, *11*(7), e1994. https://doi.org/10.1002/eco.1994

Maneta, M., Schnabel, S., & Jetten, V. (2008). Continuous spatially distributed simulation of surface and subsurface hydrological processes in a small semiarid catchment. *Hydrological Processes*, *22*(13), 2196–2214. https://doi.org/10.1002/hyp.6817

Maneta, M. P., & Silverman, N. L. (2013). A spatially distributed model to simulate water, energy, and vegetation dynamics using information from regional climate models. *Earth Interactions*, *17*(11), 1–44. https://doi.org/10.1175/2012EI000472.1

Martin, J., Looker, N., Hoylman, Z., Jencso, K., & Hu, J. (2017). Hydrometeorology organizes intra-annual patterns of tree growth across time, space and species in a montane watershed. *New Phytologist*, *215*(4), 1387–1398. https://doi.org/10.1111/nph.14668

Maxwell, R. M., Chow, F. K., & Kollet, S. J. (2007). The groundwater–land-surface–atmosphere connection: Soil moisture effects on the atmospheric boundary layer in fully-coupled simulations. *Advances in Water Resources*, *30*(12), 2447–2466. https://doi.org/10.1016/j.advwatres.2007.05.018

McCulloch, C. E., & Neuhaus, J. M. (2001). *Generalized linear mixed models*. Hoboken, New Jersey: John Wiley & Sons, Ltd.

McDonnell, J. J., Sivapalan, M., Vaché, K., Dunn, S., Grant, G., Haggerty, R., et al. (2007). Moving beyond heterogeneity and process complexity: A new vision for watershed hydrology. *Water Resources Research*, *43*, W07301. https://doi.org/10.1029/2006WR005467

McGuire, K. J., & McDonnell, J. J. (2010). Hydrological connectivity of hillslopes and streams: Characteristic time scales and nonlinearities. *Water Resources Research*, *46*, W10543. https://doi.org/10.1029/2010WR009341

McGuire, K. J., McDonnell, J. J., Weiler, M., Kendall, C., McGlynn, B. L., Welker, J. M., & Seibert, J. (2005). The role of topography on catchment-scale water residence time. *Water Resources Research*, *41*, W05002. https://doi.org/10.1029/2004WR003657

McLaughlin, B. C., Ackerly, D. D., Klos, P. Z., Natali, J., Dawson, T. E., & Thompson, S. E. (2017). *Hydrologic refugia, plants, and climate change*. Global change biology, (Vol. 23, pp. 2941–2961). https://doi.org/10.1111/gcb.13629

McNamara, J. P., Chandler, D., Seyfried, M., & Achet, S. (2005). Soil moisture states, lateral flow, and streamflow generation in a semi-arid, snowmelt-driven catchment. *Hydrological Processes*, *19*(20), 4023–4038. https://doi.org/10.1002/hyp.5869

Mesinger, F., DiMego, G., Kalnay, E., Mitchell, K., & Coauthors (2006). North American Regional Reanalysis. *Bulletin of the American Meteorological Society*, *87*(3), 343–360. https://doi.org/10.1175/BAMS-87-3-343

Minder, J. R., Mote, P. W., & Lundquist, J. D. (2010). Surface temperature lapse rates over complex terrain: Lessons from the Cascade Mountains. *Journal of Geophysical Research*, *115*, D14122. https://doi.org/10.1029/2009JD013493

Mohanty, B. P., & Skaggs, T. H. (2001). Spatio-temporal evolution and time-stable characteristics of soil moisture within remote sensing footprints with varying soil, slope, and vegetation. *Advances in Water Resources*, *24*(9–10), 1051–1067. https://doi.org/10.1016/S0309-1708(01)00034-3

Montgomery, D. R., & Dietrich, W. E. (2002). Runoff generation in a steep, soil-mantled landscape. *Water Resources Research*, *38*(9), 1168. https://doi.org/10.1029/2001WR000822

Moore, I. D., Grayson, R. B., & Ladson, A. R. (1991). Digital terrain modelling: A review of hydrological, geomorphological, and biological applications. *Hydrological Processes*, *5*(1), 3–30. https://doi.org/10.1002/hyp.3360050103

Morelli, T. L., Daly, C., Dobrowski, S. Z., Dulen, D. M., Ebersole, J. L., Jackson, S. T., et al. (2016). Managing climate change refugia for climate adaptation. *PLoS ONE*, *11*(8), e0159909. https://doi.org/10.1371/journal.pone.0159909

Mosley, M. P. (1982). Subsurface flow velocities through selected forest soils, South Island, New Zealand. *Journal of Hydrology*, *55*(1–4), 65–92. https://doi.org/10.1016/0022-1694(82)90121-4

Nippgen, F., McGlynn, B. L., & Emanuel, R. E. (2015). The spatial and temporal evolution of contributing areas. *Water Resources Research*, *51*, 4550–4573. https://doi.org/10.1002/2014WR016719

Nychka, D., Furrer, R., Paige, J., & Sain, S. (2017). Fields: Tools for spatial data. 2015. URL http://CRAN. R-project. org/package= fields. R package version, 7.

Oliphant, A. J., Spronken-Smith, R. A., Sturman, A. P., & Owens, I. F. (2003). Spatial variability of surface radiation fluxes in mountainous terrain. *Journal of Applied Meteorology*, *42*(1), 113–128. https://doi.org/10.1175/1520-0450(2003)042<0113:SVOSRF>2.0.CO;2

Penna, D., Tromp-van Meerveld, H. J., Gobbi, A., Borga, M., & Dalla Fontana, G. (2011). The influence of soil moisture on threshold runoff generation processes in an alpine headwater catchment. *Hydrology and Earth System Sciences*, *15*(3), 689–702. https://doi.org/10.5194/hess-15-689-2011

Raz-Yaseef, N., Yakir, D., Schiller, G., & Cohen, S. (2012). Dynamics of evapotranspiration partitioning in a semi-arid forest as affected by temporal rainfall patterns. *Agricultural and Forest Meteorology*, *157*, 77–85. https://doi.org/10.1016/j.agrformet.2012.01.015

Renner, M., Hassler, S. K., Blume, T., Weiler, M., Hildebrandt, A., Guderle, M., et al. (2016). Dominant controls of transpiration along a hillslope transect inferred from ecohydrological measurements and thermodynamic limits. *Hydrology and Earth System Sciences*, *20*(5), 2063–2083. https://doi.org/10.5194/hess-20-2063-2016

Rinderer, M., Van Meerveld, H. J., & Seibert, J. (2014). Topographic controls on shallow groundwater levels in a steep, prealpine catchment: When are the TWI assumptions valid? *Water Resources Research*, *50*, 6067–6080. https://doi.org/10.1002/2013WR015009

Rodriguez-Iturbe, I. (2000). Ecohydrology: A hydrologic perspective of climate-soil-vegetation dynamics. *Water Resources Research*, *36*(1), 3–9. https://doi.org/10.1029/1999WR900210

Roe, G. H. (2005). Orographic precipitation. *Annual Review of Earth and Planetary Sciences*, *33*(1), 645–671. https://doi.org/10.1146/annurev.earth.33.092203.122541

Rolland, C. (2003). Spatial and seasonal variations of air temperature lapse rates in Alpine regions. *Journal of Climate*, *16*(7), 1032–1046. https://doi.org/10.1175/1520-0442(2003)016<1032:SASVOA>2.0.CO;2

Rowell, E., Seielstad, C., Goodburn, J., & Queen, L. (2009, October). Estimating plot-scale biomass in a western North American mixed-conifer forest from lidar-derived tree stems. In Proc. SilviLaser Conf (pp. 14-16).

Royer, P. D., Breshears, D. D., Zou, C. B., Villegas, J. C., Cobb, N. S., & Kurc, S. A. (2012). Density-dependent ecohydrological effects of piñon–juniper woody canopy cover on soil microclimate and potential soil evaporation. *Rangeland Ecology & Management*, *65*(1), 11–20. https://doi.org/10.2111/REM-D-11-00007.1

Ruel, J. C., Pin, D., & Cooper, K. (1998). Effect of topography on wind behaviour in a complex terrain. *Forestry: An International Journal of Forest Research*, *71*(3), 261–265. https://doi.org/10.1093/forestry/71.3.261

Seibert, J., Bishop, K., Rodhe, A., & McDonnell, J. J. (2003). Groundwater dynamics along a hillslope: A test of the steady state hypothesis. *Water Resources Research*, *39*(1), 1014. https://doi.org/10.1029/2002WR001404

Seibert, J., & McGlynn, B. L. (2007). A new triangular multiple flow direction algorithm for computing upslope areas from gridded digital elevation models. *Water Resources Research*, *43*, W04501. https://doi.org/10.1029/2006WR005128

Shevenell, L. (1999). Regional potential evapotranspiration in arid climates based on temperature, topography and calculated solar radiation. *Hydrological Processes*, *13*(4), 577–596. https://doi.org/10.1002/(SICI)1099-1085(199903)13:4<577::AID-HYP757>3.0.CO;2-P

Sidle, R. C., Tsuboyama, Y., Noguchi, S., Hosoda, I., Fujieda, M., & Shimizu, T. (2000). Stormflow generation in steep forested headwaters: A linked hydrogeomorphic paradigm. *Hydrological Processes*, *14*(3), 369–385. https://doi.org/10.1002/(SICI)1099-1085(20000228)14:3<369::AID-HYP943>3.0.CO;2-P

Sperry, J. S., Stiller, V., & Hacke, U. G. (2003). Xylem hydraulics and the soil–plant–atmosphere continuum. *Agronomy Journal*, *95*(6), 1362–1370. https://doi.org/10.2134/agronj2003.1362

Swetnam, T. L., Brooks, P. D., Barnard, H. R., Harpold, A. A., & Gallo, E. L. (2017). Topographically driven differences in energy and water constrain climatic control on forest carbon sequestration. *Ecosphere*, *8*(4). https://doi.org/10.1002/ecs2.1797

Tague, C., Heyn, K., & Christensen, L. (2009). Topographic controls on spatial patterns of conifer transpiration and net primary productivity under climate warming in mountain ecosystems. *Ecohydrology*, *2*(4), 541–554. https://doi.org/10.1002/eco.88

Tenenbaum, D. E., Band, L. E., Kenworthy, S. T., & Tague, C. L. (2006). Analysis of soil moisture patterns in forested and suburban catchments in Baltimore, Maryland, using high-resolution photogrammetric and LIDAR digital elevation datasets. *Hydrological Processes*, *20*(2), 219–240. https://doi.org/10.1002/hyp.5895

Tetens, O. (1930). Uber einige meteorologische Begriffe. *Zeitschrift für Geophysik*, *6*, 297–309.

Thornthwaite, C. W. (1948). An approach toward a rational classification of climate. *Geographical Review*, *38*(1), 55–94. https://doi.org/10.2307/210739

Topp, G. C., Davis, J. L., & Annan, A. P. (1980). Electromagnetic determination of soil water content: Measurements in coaxial transmission lines. *Water Resources Research*, *16*(3), 574–582. https://doi.org/10.1029/WR016i003p00574

Torres, R., Dietrich, W. E., Montgomery, D. R., Anderson, S. P., & Loague, K. (1998). Unsaturated zone processes and the hydrologic response of a steep, unchanneled catchment. *Water Resources Research*, *34*(8), 1865–1879. https://doi.org/10.1029/98WR01140

Troch, P. A., Carrillo, G. A., Heidbüchel, I., Rajagopal, S., Switanek, M., Volkmann, T. H., & Yaeger, M. (2009). Dealing with landscape heterogeneity in watershed hydrology: A review of recent progress toward new hydrological theory. *Geography Compass*, *3*(1), 375–392. https://doi.org/10.1111/j.1749-8198.2008.00186.x

Troch, P. A., Paniconi, C., & van Loon, E. E. (2003). Hillslope-storage Boussinesq model for subsurface flow and variable source areas along complex hillslopes: 1 Formulation and characteristic response. *Water Resources Research*, *39*(11), 1316. https://doi.org/10.1029/2002WR001728

Tromp-van Meerveld, H. J., & McDonnell, J. J. (2005). Comment to "Spatial correlation of soil moisture in small catchments and its relationship to dominant spatial hydrological processes, Journal of Hydrology 286: 113–134". *Journal of Hydrology*, *303*(1–4), 307–312. https://doi.org/10.1016/j.jhydrol.2004.09.002

Tromp-van Meerveld, H. J., Seibert, J., & Peters, N. E. (2015). Hillslope–riparian-stream connectivity and flow directions at the Panola Mountain Research Watershed. *Hydrological Processes*, *29*(16), 3556–3574. https://doi.org/10.1002/hyp.10508

U.S. Department of Agriculture, National Cooperative Soil Survey. (2001). Official soil series descriptions: Lubrecht Series (Revision No. NRS-CNG-JAL). Retrieved from https://soilseries.sc.egov.usda.gov/OSD_Docs/L/LUBRECHT.html

Venables, W. N., & Ripley, B. D. (2002). *Modern applied statistics with S*, (4th ed.). New York: Springer. https://doi.org/10.1007/978-0-387-21706-2

Vivoni, E. R., Gutiérrez-Jurado, H. A., Aragón, C. A., Méndez-Barroso, L. A., Rinehart, A. J., Wyckoff, R. L., et al. (2007). Variation of hydrometeorological conditions along a topographic transect in northwestern Mexico during the North American monsoon. *Journal of Climate*, *20*(9), 1792–1809. https://doi.org/10.1175/JCLI4094.1

Wagenmakers, E. J., & Farrell, S. (2004). AIC model selection using Akaike weights. *Psychonomic Bulletin & Review*, *11*(1), 192–196. https://doi.org/10.3758/BF03206482

Western, A. W., Blöschl, G., & Grayson, R. B. (1998). Geostatistical characterisation of soil moisture patterns in the Tarrawarra catchment. *Journal of Hydrology*, *205*(1–2), 20–37. https://doi.org/10.1016/S0022-1694(97)00142-X

Western, A. W., Grayson, R. B., Blöschl, G., Willgoose, G. R., & McMahon, T. A. (1999). Observed spatial organization of soil moisture and its relation to terrain indices. *Water Resources Research*, *35*(3), 797–810. https://doi.org/10.1029/1998WR900065

Western, A. W., Zhou, S. L., Grayson, R. B., McMahon, T. A., Blöschl, G., & Wilson, D. J. (2004). Spatial correlation of soil moisture in small catchments and its relationship to dominant spatial hydrological processes. *Journal of Hydrology*, *286*(1–4), 113–134. https://doi.org/10.1016/j.jhydrol.2003.09.014

Weyman, D. R. (1973). Measurements of the downslope flow of water in a soil. *Journal of Hydrology*, *20*(3), 267–288. https://doi.org/10.1016/0022-1694(73)90065-6

Williams, C. J., McNamara, J. P., & Chandler, D. G. (2009). Controls on the temporal and spatial variability of soil moisture in a mountainous landscape: The signature of snow and complex terrain. *Hydrology and Earth System Sciences*, *13*(7), 1325–1336. https://doi.org/10.5194/hess-13-1325-2009

Woods, R. (2003). The relative roles of climate, soil, vegetation and topography in determining seasonal and long-term catchment dynamics. *Advances in Water Resources*, *26*(3), 295–309. https://doi.org/10.1016/S0309-1708(02)00164-1

Woods, R., & Rowe, L. (1996). The changing spatial variability of subsurface flow across a hillside. *Journal of Hydrology New Zealand*, *35*(1), 51–86.

Woods, R. A., Sivapalan, M., & Robinson, J. S. (1997). Modeling the spatial variability of subsurface runoff using a topographic index. *Water Resources Research*, *33*(5), 1061–1073. https://doi.org/10.1029/97WR00232

Yoshino, M. M. (1984). Thermal belt and cold air drainage on the mountain slope and cold air lake in the basin at quiet, clear night. *GeoJournal*, *8*(3), 235–250. https://doi.org/10.1007/BF00446473

Zhang, Y., Wei, H., & Nearing, M. A. (2011). Effects of antecedent soil moisture on runoff modeling in small semiarid watersheds of southeastern Arizona. *Hydrology and Earth System Sciences*, *15*(10), 3171–3179. https://doi.org/10.5194/hess-15-3171-2011